Lithos 200–201 (2014) 126–141

Contents lists available at ScienceDirect

Lithos

journal homepage: www.elsevier.com/locate/lithos

Geochemical constraints on the petrogenesis of the Salinian arc, central California: Implications for the origin of intermediate magmas

Alan D. Chapman [a,b,*], Mihai N. Ducea [b,c], Steven Kidder [d], Lucian Petrescu [c]

[a] Department of Geological Sciences and Engineering, Missouri University of Science and Technology, Rolla, MO, USA
[b] Department of Geosciences, University of Arizona, Tucson, AZ, USA
[c] University of Bucharest, Department of Geology and Geophysics, Bucharest, Romania
[d] Deptartment of Earth and Atmospheric Science, City College of New York, New York, NY, USA

A R T I C L E I N F O

Article history:
Received 21 November 2013
Accepted 17 April 2014
Available online 2 May 2014

Keywords:
Continental arc magmatism
Batholithic root
Downward host rock transport
Salinian block
California

A B S T R A C T

Magmatic arcs are the primary locations where continental crust is distilled to an intermediate, calc-alkaline composition. The root zones of continental arcs are thought to be the primary sites of magmatic differentiation, yet few deeply exhumed arc sections are available for direct study. The Coast Ridge Belt of central coastal California provides an exceptional opportunity to directly observe the cumulative effects of melting, mixing, assimilation, and homogenization related to construction of the Latest Cretaceous California arc. We present new major and trace element chemistry, as well as radiogenic isotopic ratios determined on Coast Ridge Belt assemblages representative of 20 to 30 km crustal levels. Late Cretaceous (ca. 93 to 81 Ma) gabbro, diorite, tonalite, and granodiorite of the Coast Ridge Belt are calc-alkaline, some exhibit cumulate characteristics, and all show enriched isotopic compositions ($Sr_i = 0.7061$ to 0.7092 and $\varepsilon_{Nd} = +1.4$ to -5.9). Rare earth element patterns in igneous and metaigneous rocks of the Coast Ridge Belt suggest that they are sourced deeper than the ~25 km paleodepth of the exposed section, but probably not significantly below 40 km. Underplating of basaltic melts derived from evolved lithospheric mantle provides the most satisfactory mechanism explaining geochemical and field evidence for partial melting and assimilation of metasedimentary framework rocks to yield gabbroic to dioritic magmas, followed soon thereafter by remelting to produce more silicic magmas. We suggest that basaltic underplating provided a source of heat to the base of the Salinian crust, leading to thermal weakening and downward flow of melt-fertile intra-arc supracrustal assemblages, thereby igniting the magmatic pulse that formed the Salinian arc.

1. Introduction

The upper 20–30 km of mature continental arcs found along the western margin of the Americas is characterized by intermediate compositions comparable to that of average continental crust (e.g., Cecil et al., 2012; Christensen and Mooney, 1995; Ducea, 2002; Gaschnig et al., 2011; Girardi et al., 2012; Gromet and Silver, 1987; Holland et al., 2013; Mamani et al., 2010; Matzel et al., 2006; Rudnick and Gao, 2003; Silver and Chappell, 1988; Wetmore and Ducea, 2011). The tonalitic to granodioritic bulk composition of batholiths is thought to result from interaction between basaltic mantle melts and more felsic pre-existing crust within the deep crustal roots of arcs (Hildreth and Moorbath, 1988; Rudnick, 1995; Wyllie, 1984). However, the nature of how mantle and crustal components interact within arcs remains poorly understood, due in part to the rarity of exhumed arc roots in the geologic record. Such exposures are rare in the Andes (Otamendi et al., 2012) and few examples exist in the North American Cordillera, and are limited to the North Cascades core (e.g., Miller et al., 2009; Paterson et al., 2011), the Coast Mountains batholith (Barker and Arth, 1984; Girardi et al., 2012), and the southern Sierra Nevada batholith and adjacent areas (Barth and May, 1992; Chapman et al., 2012; Kidder et al., 2003; Pickett and Saleeby, 1993; Saleeby et al., 2007).

Investigations of arc root zones are also important for understanding episodes of high-flux magmatism (Coleman and Glazner, 1998; DeCelles et al., 2009; Ducea, 2001; Ducea and Barton, 2007). High-magmatic flux events apparently correspond with periods of crustal thickening (e.g., DeCelles, 2004). Furthermore, isotopic studies (e.g., Ducea, 2001; Ducea and Barton, 2007) indicate that more than half of the magmatic mass added to arcs in flare-up mode must be crust- (i.e., not mantle) derived. Therefore, simultaneous crustal thickening and delivery of supracrustal material to the arc magma source provide an elegant explanation for magmatic flare-ups. What processes are capable of thickening the crust while also transferring supracrustal assemblages into the roots of continental arcs? End-member possibilities include: downward flow of upper crustal sections (Babeyko et al., 2002; Paterson and Farris, 2008; Saleeby, 1990), subduction erosion and tectonic underplating from the trench side (Ducea et al., 2009; Kay et al., 2005; Stern, 1991; von Huene and Scholl, 1991), retroarc

* Corresponding author at: Department of Geological Sciences and Engineering, Missouri University of Science and Technology, Rolla, MO, USA. Tel.: +1 573 341 4100.
E-mail address: chapmanad@mst.edu (A.D. Chapman).

http://dx.doi.org/10.1016/j.lithos.2014.04.011
0024-4937/

thrusting from the foreland (e.g., Chin et al., 2013; DeCelles et al., 2009; Ducea, 2001), and detachment and buoyant ascent from the downgoing plate (Behn et al., 2011; Chapman et al., 2013; Hacker et al., 2011). The California arc (Fig. 1), comprising Salinia, the Mojave Desert, and Sierra Nevada and Peninsular Ranges batholiths, provides an excellent opportunity to test between the mechanisms listed above, given the well-exposed and understood relationships between plutons, pre-intrusive framework rocks, and subduction accretion assemblages.

We present new major and trace element chemistry, as well as Sr and Nd isotopic ratios of 18 intrusive rocks, four framework metasedimentary rocks, and four mafic bodies from the Coast Ridge Belt (CRB), a deep exposure of the Late Cretaceous California arc in the

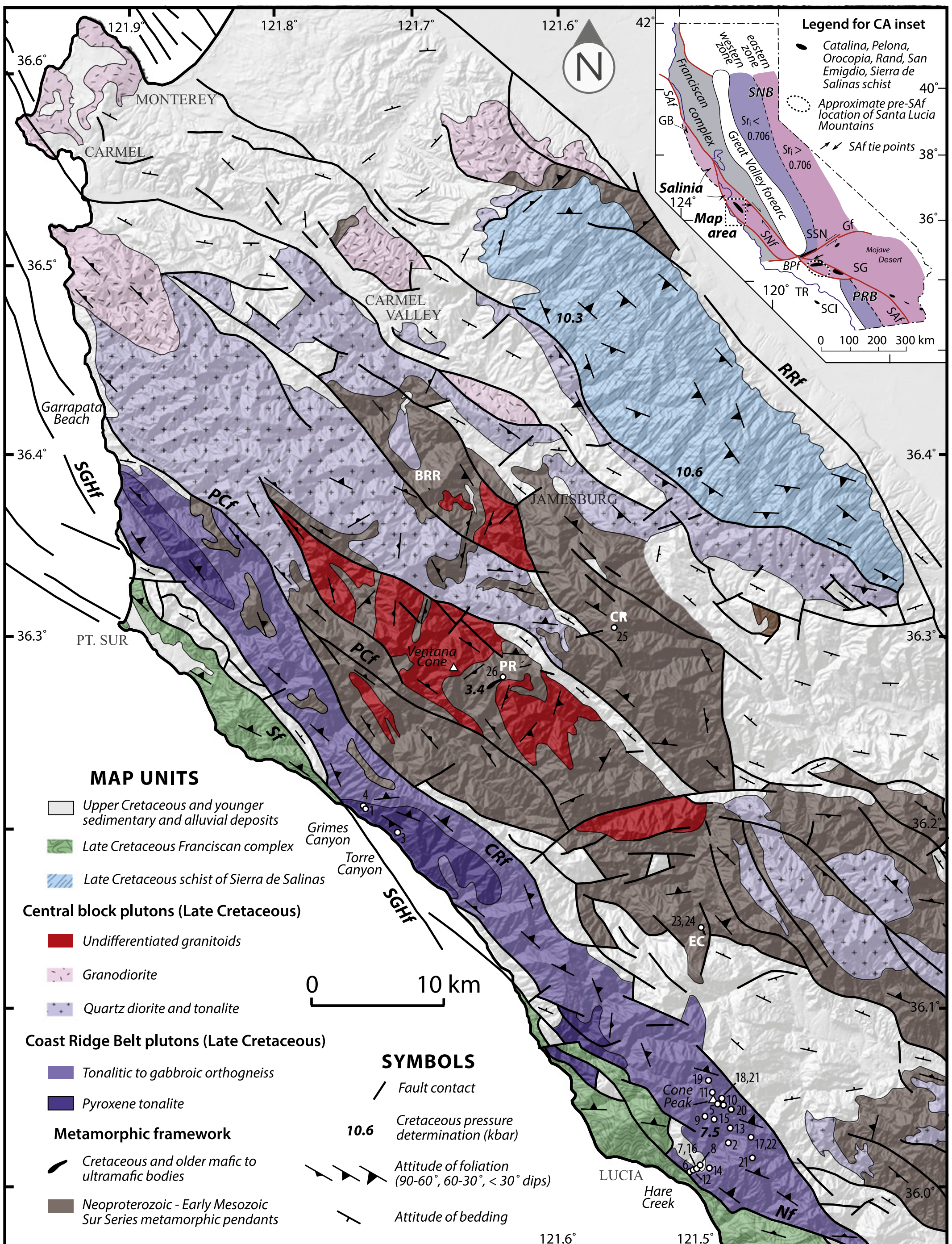

Fig. 1. Geologic map of the northern Santa Lucia Range draped over a DEM and showing geochemical sample locations. Geologic and structural data from Compton (1960, 1966), Wiebe (1966, 1970), Ross (1972, 1975, 1978, 1979), Nutt (1977), Bush (1981), and Hall (1991). Pressure determinations from Kidder et al. (2003), Kidder and Ducea (2006), and Chapman et al. (2012). Magmatic and solid state foliations are not distinguished for simplicity; foliations in Central block plutons are generally magmatic and those shown for the Sur Series, schist of Sierra de Salinas, and Coast Ridge belt are generally solid state. Abbreviations of small Salinian ultramafic-mafic bodies: BRR, Blue Rock Ridge; CR, Chews Ridge; EC, Escondido complex; PR, Pine Ridge. Inset shows location of Salinian terrane and related elements of the California arc (shown in purple and pink). Fault abbreviations: BPf, Big Pine; CRf, Coast Ridge; Gf, Garlock; Nf, Nacimiento; PCf, Palo Colorado; RRf, Reliz-Rinconada; Sf, Sur; SAf, San Andreas; SGHf; San Gregorio-Hosgri; SNf, Sur-Nacimiento. Other inset abbreviations: PRB, Peninsular Ranges batholith; SCI, Santa Catalina Island; SNB; Sierra Nevada batholith; SSN, southern Sierra Nevada.

Santa Lucia Range (Compton, 1960, 1966; Ducea et al., 2003a; Kidder et al., 2003; Kistler and Champion, 2001; Mattinson, 1978, 1990; Wiebe, 1970). This effort builds upon previously published geologic, geochemical, geochronologic, and thermobarometric data sets, thereby providing a new framework for understanding the petrogenetic and tectonic processes that built the roots of the Salinian arc. The purpose of this investigation is two-fold: 1) to provide geochemical constraints on how the magma depths and sources evolved during construction of the Coast Ridge belt and to compare these results with other batholithic root zones exposed in the North American Cordillera and 2) to better understand how supracrustal rocks are incorporated into continental arcs and how the input of these materials may influence magma productivity and composition.

2. Geologic background

2.1. Salinia and the Coast Ridge Belt

The Salinian block of central coastal California (e.g., Vedder et al., 1982) is a NW-trending composite terrane bounded to the east by the San Andreas fault, to the west by the Sur-Nacimiento fault, and to the south by the Big Pine fault (Fig. 1). These faults juxtapose the Salinian block to the west and east with Mesozoic subduction accretion assemblages of the Franciscan complex (Fig. 1). The Salinian terrane traveled northward >300 km during the Neogene along the San Andreas fault system (Dickinson et al., 2005; Hall, 1991; Hall and Saleeby, 2013; Huffman, 1972; Jacobson et al., 2011; Matthews, 1976; Page, 1982; Schott and Johnson, 1998; Sharman et al., 2013; Fig. 1). Petrologic, isotopic, geochronologic, structural, and sedimentologic evidence places Salinia near the southern end of the Sierra Nevada batholith in Late Cretaceous time (Barbeau et al., 2005; Chapman et al., 2012; Hall, 1991; Hall and Saleeby, 2013; James, 1992; Kistler and Peterman, 1978; Sharman et al., 2013; Wood and Saleeby, 1997; Fig. 1 inset). When slip along the San Andreas fault is removed, plutonic rocks of the Sierra Nevada, Salinian, Mojave, and Peninsular Ranges blocks form a contiguous ~1500 km long, NNW-trending Mesozoic batholith, referred to here as the California arc.

Three main rock packages underlie the Santa Lucia Range of central Salinia, discussed in the following order below: Paleozoic metamorphic framework rocks, Late Cretaceous plutonic rocks, and subduction accretion assemblages. First, Paleozoic upper amphibolite to granulite grade assemblages of the "Sur Series" (Barbeau et al., 2005; Compton, 1960, 1966; James and Mattinson, 1988; Trask, 1926; Wiebe, 1970) form the framework for Cretaceous intrusives of the Salinian arc. The Sur Series comprises interlayered graphitic quartzofeldspathic gneiss and schist, psammite, marble, amphibolite, calc-silicate, and silicic metavolcanic rocks (Ross, 1978), interpreted as highly metamorphosed and deformed clastic strata of the Cordilleran passive margin (Barbeau et al., 2005; Chapman et al., 2012; Compton, 1960, 1966; Kidder et al., 2003; Mattinson, 1978). At least fifty small (<1 km diameter), mafic to ultramafic bodies crop out entirely within Sur Series meta-sedimentary rocks (Fig. 1; Bush, 1981; Nutt, 1977; Wiebe, 1966, 1970); Chews Ridge, Pine Ridge, and Escondido bodies are among those least altered. Chews Ridge and Pine Ridge bodies are variably serpentinized and elongated parallel to the foliation of Sur Series assemblages. In contrast, the Escondido body exhibits primary igneous characteristics, including orthocumulate textures (Fig. 2A), and crosscuts Sur Series fabrics.

The Sur Series is intruded by Late Cretaceous intermediate to mafic plutons of the Salinian magmatic arc (Compton, 1960; Hansen and Harlov, 2009; Hansen and Stuk, 1993; Kidder et al., 2003; Mattinson, 1978, 1990; Wiebe, 1970). Magmatism began in the Salinian arc at ca. 100 Ma and continued until ca. 80 Ma (Kistler and Champion, 2001; Mattinson, 1978, 1990). The bulk of the section was constructed between ca. 93 and 81 Ma (Kidder et al., 2003) during an episode of high flux magmatism that produced >80% of the California arc (Coleman and Glazner, 1998; DeCelles et al., 2009; Ducea, 2001; Ducea and Barton, 2007). Plutonic assemblages of the Salinian arc range in compositions from quartz monzonite and granodiorite to tonalite, quartz diorite, diorite, and gabbro (Mattinson, 1978; Ross, 1972). The depth of exposure increases from east to west in the Salinian arc from mesozonal in the Gabilan and eastern Santa Lucia ranges (~3 to 6 kbar; Chapman et al., 2012; John, 1981; Wiebe, 1970) to ~7.5 kbar levels (Hansen and Stuk, 1993; Kidder et al., 2003) in the CRB west of the Coast Ridge and Palo Colorado faults along the western flank of the Santa Lucia Mountains (Fig. 1). Shallower-level Salinian arc assemblages east of the CRB are referred to as the Central block (Ross, 1978).

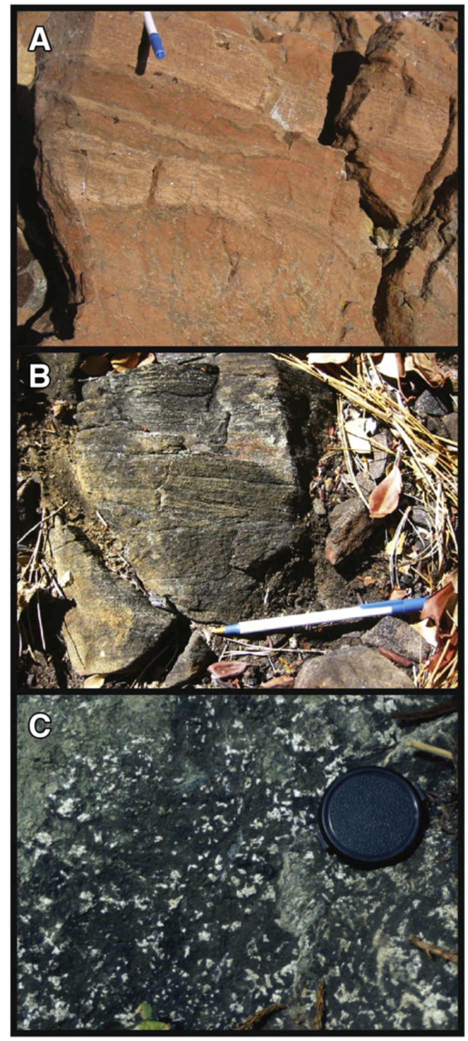

Fig. 2. Orthocumulate textures in rocks of the (A) Escondido body (layering defined by weathered olivine-rich and relatively resistant orthopyroxene, clinopyroxene, and amphibole-rich bands) and (B) Group 2B (layering defined by hornblende- and plagioclase-rich bands) and (C) Group 1A (note dark hornblende and light plagioclase phenocrysts) of the CRB.

Compositional and structural observations (Ducea et al., 2003a; Kidder et al., 2003) suggest that the CRB represents a window into the root of a continental arc (Hildreth and Moorbath, 1988). The amount of mafic material in the CRB is significantly higher than that in the Central block, suggesting that the CRB was an accumulation site for Late Cretaceous mafic magmas ascending from the mantle. Furthermore, tilt-corrected (Kidder et al., 2003) plutonic and metamorphic fabrics exhibit a gradual transition from subvertical in the Central block, to subhorizontal in the CRB. This observation has been interpreted previously (Kidder et al., 2003) to reflect vertical transport of upper crustal material into the lower crust, where it spread laterally as a gravity current. Therefore, the CRB may represent a zone of mixing of mantle-derived magmas and downward flowing supracrustal assemblages.

Mid-crustal plutons of the Central block structurally overlie the Late Cretaceous schist of Sierra de Salinas along the Salinas shear zone, a Late Cretaceous low angle normal fault responsible for the exhumation of the schist (Barth et al., 2003; Chapman et al., 2010; 2011; 2013; Kidder and Ducea, 2006; Kidder et al., 2013; Fig. 1). The schist of Sierra de Salinas and related schists of southern California (e.g., Jacobson et al., 2011 and references therein) are trench-related subduction accretion assemblages that were deposited in the Late Cretaceous trench and underplated directly beneath the California arc during an episode of shallow subduction related to the Laramide orogeny (Ducea et al., 2009).

2.2. Sample petrography

Basement samples were collected throughout the CRB, from which twenty-two relatively unaltered samples from Cone Peak, Grimes Canyon, and Torre Canyon areas were selected for whole rock major, trace element, rare-earth element, and isotopic analyses (Fig. 1). Samples from the Cone Peak vicinity were collected along Hare Creek and Vicente Flat trails and from near Cone Peak. All rock types found in the CRB are represented in the samples identified here; therefore, the data presented herein is thought to adequately represent the geochemistry of the CRB as a whole. Care was taken to avoid sampling centimeter-scale leucocratic veins and biotite rich zones, interpreted by Hansen and Stuk (1993) as the products of local partial melting of the Sur Series metamorphic framework. Clinopyroxene and hornblende grains from an additional four samples of mafic and ultramafic rock from Escondido, Chews Ridge, and Pine Ridge bodies (Fig. 1) were separated from whole rock crushes using standard magnetic, heavy liquid, and handpicking techniques and analyzed for Sr and Nd isotopes. Whole rock analyses were not attempted for this suite given the high degree of alteration of these rocks. Escondido and Chews Ridge separates are mostly inclusion-free, whereas clinopyroxene grains from the Pine Ridge body contain inclusions of ilmenite.

The reader is referred to Compton (1960, 1966), Ross (1979), Hansen and Stuk (1993), Kidder et al. (2003), and Hansen and Harlov (2009) for detailed petrographic descriptions of rocks from Cone Peak and Grimes-Torre canyons areas and to Wiebe (1966, 1970), Nutt (1977), and Bush (1981) for descriptions of mafic-ultramafic bodies east of the Coast Ridge fault. Brief descriptions and approximate sample locations are given in Table 1. The basement rocks of the CRB are broadly divided into four groups: Group 1, Late Cretaceous mafic intrusions of quartz diorite and gabbro; Group 2, Late Cretaceous orthogneiss, including granulite and “charnockitic rocks” of Compton (1960); a third group of quartzite, marble, and garnet-bearing quartzofeldspathic schist belonging to the Sur Series; and a fourth group of late, cross-cutting quartzofeldspathic dikes. Geochronologic data and intrusive relationships

Table 1
Sample locations and descriptions.

Sample	Field name	Latitude (°N)[a]	Longitude (°W)[a]	Location	Rock type
Coast Ridge belt plutons and orthogneisses — Late Cretaceous plutons of the Salinian magmatic arc					
Group 1A — medium- to coarse-grained granoblastic cumulate gabbro					
8	814.9	36.0173	121.5033	Cone Peak	Hb mafic cumulate
9	802.6	36.0430	121.5012	Cone Peak	Hb + cpx mafic cumulate
Group 1B — fine-grained non-cumulate gabbro containing more hbl than Group 1A ± cpx ± grt					
10	709.2	36.0493	121.4891	Cone Peak	Hb + bt + grt quartz diorite
11	813.1	36.0558	121.4964	Cone Peak	Hb + bt + cpx quartz diorite
Group 1C — Cone Peak migmatitic banded gneiss					
12	814.2	36.0151	121.5076	Cone Peak	Hb + cpx gabbro
13	817.1	36.0374	121.4839	Cone Peak	Hb + grt gabbro
14	730.3	36.0156	121.4967	Cone Peak	Hb + grt amphibolite
15	813.2	36.0417	121.4950	Cone Peak	Hb + bt amphibolite
16	814.12	36.0127	121.5131	Cone Peak	Hb + cpx + bt amphibolite
Group 2A — mafic granulite with allotriomorphic texture containing opx + kfs ± grt ± hb					
1	99BS2/2	36.2036	121.7299	Grimes Canyon	Opx + cpx + grt tonalite
2	718.3	36.0291	121.4852	Cone Peak	Opx + bt + grt tonalite gneiss
Group 2B — felsic granulite associated with group 2A rocks, exhibiting similar textures but lacking opx and grt					
3	99BS1/8B	36.1950	121.7150	Torre Canyon	Hb + cpx tonalite
4	99BS2/1A	36.2052	121.7354	Grimes Canyon	Hb + cpx tonalite
Group 2C — felsic gneiss showing deformed cumulate textures					
5	808.7	36.0498	121.4930	Cone Peak	Hb + bt quartz diorite
6	630.4	36.0133	121.5104	Cone Peak	Cpx granulite gneiss
7	814.11	36.0127	121.5131	Cone Peak	Cpx granulite gneiss
Late intrusive rocks — non-deformed cross-cutting quartzofeldspathic dikes					
17	99BS1/4A	36.0337	121.4689	Cone Peak	Cpx + opx tonalite dike
18	99BS1/7A	36.0528	121.4897	Cone Peak	Trondhjemite dike
Framework metasedimentary rocks — quartzite, marble, and grt-bearing quartzofeldspathic schist					
19	711.3	36.0622	121.4986	Cone Peak	Bt + grt psammite
20	815.3B	36.0475	121.4834	Cone Peak	Bt + grt psammite
21	99BS1/7C	36.0528	121.4897	Cone Peak	Bt + grt psammite
22	99BS1/4C	36.0337	121.4689	Cone Peak	Marble
Ultramafic-mafic bodies — small lozenges within Sur Series meta-sedimentary rocks					
23H	1010-7 hbd	36.1300	121.4750	Escondido complex	Hb + cpx gabbro
23C	1010-7 cpx	36.1300	121.4750	Escondido complex	Hb + cpx gabbro
24H	bs3	36.1300	121.4750	Escondido complex	Hb peridotite
25C	1008-5 cpx	36.3130	121.5720	Chews Ridge	Clinopyroxenite
26C	31001-3 cpx	36.2770	121.6470	Pine Ridge	Clinopyroxenite

Mineral abbreviations: bt, biotite; cpx, clinopyroxene; grt, garnet; hb, hornblende; kfs, k-feldspar; opx, orthopyroxene.
[a] Locations approximate.

Table 2
Major and trace element data for Coast Ridge belt samples.

Group	Group 2A		Group 2B		Group 2C			Group 1A		Group 1B		Group 1C					Metamorphic	
Sample	1	2	3	4	5	6	7	8	9	10	11	12	13	14	15	16	19	20
Rock type	Pyroxene tonalite	Tonalite gneiss	Pyroxene tonalite	Pyroxene tonalite	Quartz diorite	Granulite gneiss	Granulite gneiss	Mafic cumulate	Mafic cumulate	Quartz diorite	Quartz diorite	Gabbro cumulate	Gabbro	Amphibolite	Amphibolite	Amphibolite	Quartzite	Quartzite
SiO_2	59.94	61.46	60.27	69.09	56.15	61.27	60.91	43.78	47.84	50.51	50.25	48.18	50.16	45.42	45.67	53.65	83.37	83.89
Al_2O_3	16.36	17.14	17.29	14.42	19.16	16.89	18.29	19.54	26.23	19.69	19.19	13.76	20.56	19.88	18.77	15.45	6.59	7.19
FeO*	9.63	7.81	7.59	3.45	4.91	8.92	5.40	11.08	3.50	10.10	10.36	9.91	9.97	11.33	11.05	8.98	6.39	3.04
MnO	0.31	0.20	0.17	0.05	0.13	0.06	0.10	0.10	0.10	0.10	0.10	0.21	0.21	0.21	0.21	0.10	0.10	0.10
MgO	2.71	2.03	2.96	0.91	4.17	2.29	3.22	6.90	5.25	3.37	3.65	8.13	3.95	7.00	6.78	7.31	1.62	1.22
CaO	5.45	5.38	5.22	7.90	7.92	5.08	5.93	13.38	14.30	8.27	7.82	15.85	8.31	11.33	10.22	9.50	0.41	0.61
Na_2O	3.37	2.84	3.89	3.40	5.05	4.17	4.14	2.30	1.44	3.88	3.86	1.88	3.22	2.16	2.61	3.03	1.01	0.61
K_2O	0.80	1.12	1.37	0.12	0.53	0.37	0.61	0.52	1.13	1.63	2.23	0.52	0.93	0.82	1.46	0.52	0.30	2.94
TiO_2	1.15	1.62	1.04	0.53	1.66	0.74	1.06	2.30	0.21	1.84	2.13	1.56	2.18	1.65	3.02	1.04	0.20	0.30
P_2O_5	0.27	0.41	0.20	0.13	0.31	0.21	0.35	0.10	0.00	0.61	0.41	0.00	0.52	0.21	0.21	0.42	0.00	0.10
A/CNK	1.00	1.10	0.99	0.72	0.82	1.02	1.00	0.68	0.89	0.85	0.84	0.42	0.96	0.79	0.77	0.68	2.41	1.36
Mg#	36	34	44	34	63	34	54	55	75	40	41	62	44	55	55	62	33	44
Sc	34.8	13.3	17.6	9.8	14.1	4.9	5.2	36.2	15.7	19.4	16.6	42.5	18.0	32.7	29.0	29.8	15.1	10.4
V	128	65	112	48	178	83	115	457	66	55	131	366	183	260	434	205	26	50
Cr	14	156	9	4	4	37	20	19	140	100	42	33	65	139	41	152	1020	342
Co	15	10	18	7	21	12	9	38	15	16	19	32	21	35	40	26	10	9
Ni	6	3	4	1	16.5	1	1.1	9	10	2	1	11	9	7	4	22	27	36
Cu	13	7	11	5	10	11.5	20.2	19	13	13	12	16	15	13	3	34	23	21
Zn	147	111	129	60	119.7	122.6	177.5	49	34	133	141	75	100	106	90	156	51	59
Rb	15.0	20.1	66.1	3.0	10.0	17.0	16.0	9.8	29.3	66.5	50.7	6.1	16.7	8.7	47.0	17.9	10.0	51.0
Sr	411.0	299.6	501.2	102.3	619.0	889.0	833.0	675.6	448.5	557.6	472.0	475.8	715.6	495.6	550.0	477.0	61.0	116.0
Y	85	33	12	13	6	3	5	13	2	41	30	17	21	26	19	18	50	17
Zr	346	227	140	120	15	202	146	34	17	461	220	62	230	65	75	119	166	80
Ba	449	799	547	90	438	270	507	277	625	839	1096	226	406	281	521	434	51	3522
La	16.9	26.4	14.5	13.3	13.6	9.2	9.8	4.3	1.9	40.3	19.2	5.6	13.3	6.8	6.9	19.4	16.0	17.9
Ce	36	52	26	22	23	13	16	10	4	85	45	15	32	19	18	45	38	30
Nd	21.0	28.0	18.1	12.0	11.0	10.0	8.0	6.8	3.0	62.9	41.3	12.6	20.0	15.6	14.0	30.0	13.0	12.0
Sm	6.5	7.2	4.0	3.1	2.1	1.4	1.7	2.1	0.6	14.2	9.7	3.6	5.0	4.4	3.9	6.5	2.7	2.8
Eu	1.3	1.9	0.9	1.0	1.4	1.4	1.3	1.1	0.4	3.0	2.2	1.1	1.5	1.5	1.4	1.5	0.4	1.0
Tb	1.5	0.9	0.1	0.2	0.1	0.2	0.2	0.2	0.2	1.5	1.0	0.6	0.2	0.6	0.7	0.6	0.7	0.1
Yb	9.2	2.9	1.0	1.0	0.4	0.3	0.3	1.2	0.3	2.8	2.1	1.8	2.1	2.8	1.5	1.6	8.9	2.1
Lu	1.32	0.44	0.15	0.15	0.06	0.05	0.05	0.18	0.05	0.40	0.31	0.27	0.31	0.43	0.23	0.24	1.24	0.33
Hf	7.6	5.8	3.6	4.0	0.1	5.5	2.6	0.3	0.2	10.0	5.7	2.4	4.9	2.2	2.2	2.6	4.5	2.5
Th	0.5	2.0	0.1	0.1	0.5	0.5	0.5	0.2	0.5	1.6	0.6	0.6	0.4	0.3	1.1	0.3	8.2	6.0
U	0.3	0.3	0.5	0.3	0.5	0.5	0.3	0.3	0.6	1.0	0.2	0.7	0.5	0.4	0.1	0.3	0.8	0.2
Sr/Y	4.84	9.08	41.77	7.87	103.17	296.33	166.60	51.97	224.25	13.60	15.73	27.99	34.08	19.06	28.95	26.50	1.22	6.82
La/Yb	1.84	9.10	14.50	13.30	34.00	30.67	32.67	3.58	6.33	14.39	9.14	3.11	6.33	2.43	4.60	12.13	1.80	8.52
La/Sm	2.60	3.67	3.62	4.29	6.48	6.57	5.76	2.06	3.17	2.84	1.97	1.56	2.66	1.54	1.77	3.00	5.93	6.39
Sm/Yb	0.71	2.48	4.01	3.10	5.25	4.67	5.67	1.74	2.00	5.07	4.64	1.99	2.38	1.58	2.60	4.05	0.30	1.33
Eu/Eu*	0.53	0.91	1.07	1.31	2.93	3.29	2.69	1.98	1.46	0.77	0.83	0.95	1.35	1.14	1.08	0.88	0.37	1.64

Notes: Major elements in wt.%, normalized to 100. Trace elements in ppm. FeO* is total iron as FeO. LOI not determined.
A/CNK, $Al_2O_3/(CaO + Na_2O + K_2O)$; Mg#, molecular MgO/MgO + FeO; Eu/Eu*, Eu divided by (Sm + Tb)/2.

indicate that Groups 1 and 2 assemblages are a broadly coeval intrusive suite (Kidder et al., 2003). Groups 1 and 2 are further subdivided below.

Six distinct subsets of igneous and metaigneous samples are apparent based on textures and geochemistry. Group 2 is subdivided as follows: A) mafic granulite with allotriomorphic texture containing orthopyroxene + K-feldspar ± garnet ± hornblende; B) felsic granulite associated with (A), exhibiting similar textures but lacking orthopyroxene and garnet; and C) felsic gneiss showing deformed orthocumulate textures (Fig. 2B), interlayered with metamorphic framework rocks of the Sur Series, and ranging in composition from tonalite to diorite. Group 1 plutons are more mafic in composition than those of Group 2 and preserve hypidiomorphic granular (igneous) textures. Group 1 includes two (<200 m) texturally and compositionally heterogeneous hornblende gabbro sills south of Cone Peak. Two principal end members comprise these sills: Group 1A, a medium- to coarse-grained granoblastic orthocumulate gabbro (Fig. 2C) and Group 1B, a fine-grained non-cumulate variety containing a higher proportion of hornblende and in some cases clinopyroxene and/or garnet. A final subgroup, Group 1C, is exposed at Cone Peak and consists of migmatitic banded gneiss characterized by leucocratic veins, vein-parallel biotite-rich zones, and quartz diorite host rock (Hansen and Harlov, 2009; Hansen and Stuk, 1993). Five samples (Table 1) are characterized by coarse (~1 cm) garnet porphyroblasts that overgrow primary igneous textures. Cumulate rocks (Fig. 2) are not considered in petrogenetic interpretations presented here because they do not reflect melt compositions.

3. Analytical techniques

Whole rock samples were analyzed for major element chemistry by wavelength dispersive X-ray fluorescence and for trace element chemistry by quadrupole ICP-MS using standard techniques at Activation Laboratories. The reported uncertainties are less than 1% for the major elements and ~5% for trace elements.

Approximately 100 to 300 mg of representative whole rock (CRB suite) and mineral separate (ultramafic suite) powders were spiked with mixed ^{85}Rb–^{84}Sr and ^{149}Sm–^{150}Nd tracers. Dissolution of the spiked samples for isotopic analyses was performed in screw-cap Teflon beakers using HF–HNO_3 (on hot plates) and HF–$HClO_4$ mixtures (in open beakers at room temperature). Undissolved residues, when present, were attacked using mixtures of HF and $HClO_4$. Separation of Rb, Sr, and the bulk of the REE was achieved via HCl elution in standard cation columns (Otamendi et al., 2009; Patchett and Ruiz, 1987). Separation of Sm and Nd was carried out using LNSpec® resin following the procedures outlined in Ducea et al. (2003b) and Otamendi et al. (2009).

Mass spectrometric analyses were carried out on two VG Sector multicollector instruments (VG54 and VG354) fitted with adjustable 10^{11} Ω Faraday collectors and Daly photomultipliers (Patchett and Ruiz, 1987). Concentrations of Rb, Sr, Sm, and Nd were determined by isotope dilution, with isotopic compositions of Sr and Nd determined on the same spiked runs. An off-line manipulation program was used for isotope dilution calculations. Typical runs consisted of acquisition of 100 isotopic ratios. Four analyses of the standard NRbAAA were performed during this study, with mean $^{85}Rb/^{87}Rb = 2.61199 \pm 20$. Fifteen analyses of standard Sr987 yielded mean ratios of $^{87}Sr/^{86}Sr = 0.710285 \pm 7$ and $^{84}Sr/^{86}Sr = 0.056316 \pm 12$. The mean results of five analyses of the standard nSmβ performed during this study are $^{148}Sm/^{147}Sm = 0.74880 \pm 21$, and $^{148}Sm/^{152}Sm = 0.42110 \pm 6$. Fifteen measurements of the LaJolla Nd standard yielded the following isotopic ratios: $^{142}Nd/^{144}Nd = 1.14184 \pm 2$, $^{143}Nd/^{144}Nd = 0.511853 \pm 2$, $^{145}Nd/^{144}Nd = 0.348390 \pm 2$, and $^{150}Nd/^{144}Nd = 0.23638 \pm 2$. The Sr and Nd isotopic ratios of standards and samples were normalized to $^{86}Sr/^{88}Sr = 0.1194$ and $^{146}Nd/^{144}Nd = 0.7219$. The estimated analytical $\pm 2\sigma$ uncertainties for samples analyzed here are $^{87}Rb/^{86}Sr = 0.55\%$, $^{87}Sr/^{86}Sr = 0.0014\%$, $^{147}Nd/^{144}Nd = 0.8\%$, and $^{143}Nd/^{144}Nd = 0.002\%$. Procedural blanks averaged from five determinations were Rb: 10 pg, Sr: 150 pg, Sm: 2.7 pg, and Nd: 5.5 pg.

4. Results

4.1. Major elements

Whole rock major and trace element data are given in Table 2 for all CRB sample groups except late intrusive dikes. The bulk-rock composition of igneous samples from the CRB varies continuously from 44 to 61 wt.% SiO_2 with one outlier at 69 wt.% SiO_2. Variation diagrams of major oxides plotted against silica (Fig. 3) show three distinct clusters corresponding to the two groups of the CRB and Late Cretaceous granitoids of the Central block. Both groups of the CRB are less silicic than Central block plutons and show more scatter in major element oxide values. This scatter is probably due to the effects of crystal accumulation in Group 2C and Group 1A samples exhibiting cumulate textures, causing the bulk compositions of these rocks to plot off the liquid line of descent. Group 2 rocks are more silicic, overlap leucocratic vein compositions of Hansen and Stuk (1993), and show opposing trends in Al_2O_3 and Na_2O in Harker diagrams than Group 1, with the intersection of these trends at ~50 wt.% SiO_2. In both the CRB and the Central block, with increasing silica: TiO_2, FeO*, MgO, and CaO generally decrease and are sharply defined, MnO and Mg# (100 × molecular MgO/(MgO + FeO*)) decrease and are more scattered, K_2O decreases slightly and is dispersed, and Al_2O_3, Na_2O, and P_2O_5 exhibit diffuse convex upward shapes.

Both groups of the CRB are calcic to calc-alkalic, using the alkali-lime index of Frost et al. (2001) with eight Group 1 samples, all from Cone Peak, falling mostly within the alkali-calcic and alkali fields (Fig. 3). Rocks of the CRB have alumina saturation indices ranging from 0.4 to 1.1 (metaluminous) and plot mostly within the calc-alkaline field on an AFM diagram (Fig. 4). Rock compositions of the Central block are also mostly calc-alkalic, but are more silicic than the CRB and have alumina saturation indices extending into the peraluminous field (Fig. 3). In aggregate, rocks of the CRB and the Central block define a tholeiitic to calc-alkaline evolutionary trend with moderate iron enrichment followed by iron depletion and alkali enrichment.

4.2. Trace elements

Normal mid-ocean ridge basalt (N-MORB)-normalized trace element patterns (Fig. 5A) show similar trends for both groups of the CRB. Both groups are strongly enriched in fluid-mobile light ion lithophile elements (LILE) and have negative anomalies of high field strength elements (HFSE). The overall trace element pattern features prominent troughs in Th, peaks in Ba and K and highly variable HFSE concentrations. Group 2C, 1A, and 1B samples show an additional peak in Sr.

Plots of certain trace element concentrations versus silica content are shown in Fig. 6 for both the CRB and the Central block. Inspection of Fig. 6 reveals the following relationships: 1) compatible trace elements, including Sc, V, Co, Cr, and Ni, have higher abundances in assemblages of the CRB and show a strong negative correlation with SiO_2; 2) incompatible trace elements such as Ba and Zr increase with SiO_2; and 3) Y does not vary significantly with silica.

4.3. Rare earth elements

Chondrite-normalized rare-earth element variation patterns for intrusive assemblages of the CRB are shown in Fig. 5B. All samples show some enrichment in light rare earth elements (LREE) relative to heavy rare earth elements (HREE), resulting in moderate to steep overall REE patterns. Six distinct subsets of samples, corresponding to the subsets defined above, are apparent based on REE patterns. Group 2A and 2B granulites are more enriched in LREE than Group 1 rocks and show a

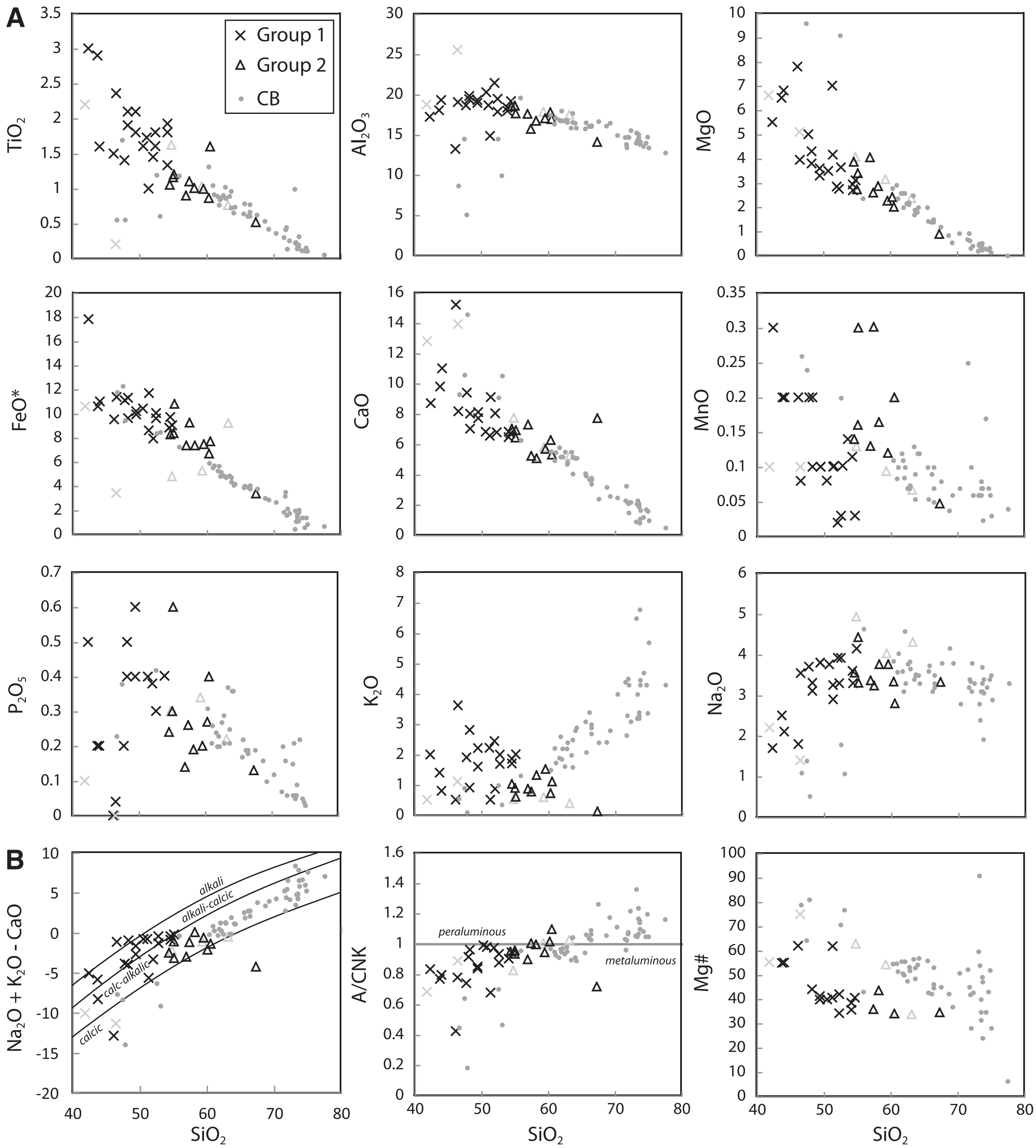

Fig. 3. (A) Major element variation diagrams for Group 1 and Group 2 samples of the CRB (Compton, 1960; Ross, 1979; Hansen and Stuk, 1993; this study) and the Central block (CB; Lawson, 1893; Compton, 1966; Ross, 1972, 1975, 1979). FeO* denotes total Fe as FeO. (B) Alkali-lime index ($Na_2O + K_2O$–CaO), alumina saturation index (molar $Al_2O_3/(CaO + Na_2O + K_2O)$, A/CNK), and Mg# (molecular MgO/MgO + FeO) versus wt.% SiO_2. Gray CRB symbols denote samples exhibiting cumulate characteristics.

wide range in HREE abundances. Two Group 2B samples exhibit negative Eu anomalies and are significantly more enriched in HREE than samples that lack Eu anomalies. Group 2C gneisses are characterized by large positive Eu anomalies and depletion in HREE relative to other groups, resulting in a steeply sloping overall REE pattern. Gabbroic samples in Group 1 exhibit a moderately sloping (La to Tb) to somewhat flat (Y to Lu) pattern. Two orthocumulate gabbro samples in Group 1A, one of which is somewhat depleted relative to the rest of the group, show positive Eu anomalies. Five samples in groups 1B and 1C display convex upward patterns with apexes at Nd. Diorite gneisses of Group 1C are enriched in LREE and MREE relative to other groups, and show small negative Eu anomalies and a flat HREE pattern from Yb to Lu.

Light rare earth elements La to Sm show a positive correlation with SiO_2, whereas heavier REE Eu to Lu do not vary significantly with SiO_2. These relations are highlighted in Fig. 6 as plots of La, Ce, Eu, and Yb versus SiO_2.

4.4. Key elemental ratios

The elemental ratios Sr/Y, La/Yb, La/Sm, and Sm/Yb are commonly used proxies for the minimum depth of melt fractionation and/or melting in intermediate, arc-related rocks since they are sensitive to the presence of fractionating garnet, which preferentially incorporates the heavy REEs, and plagioclase, which strongly concentrates Sr and

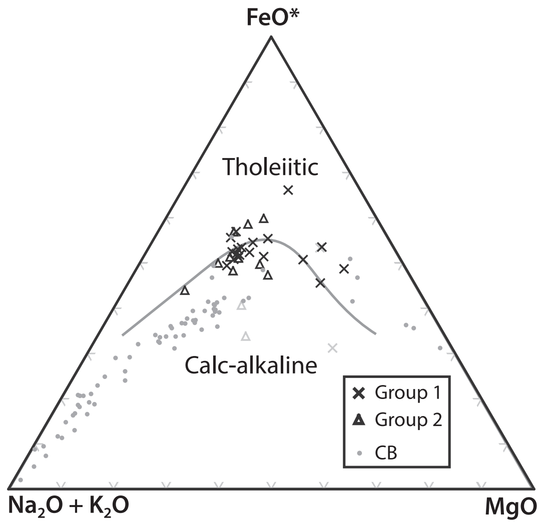

Fig. 4. AFM diagram showing that rocks of the CRB (Group 1 and Group 2) and the Central block (CB) define a tholeiitic to calc-alkaline evolutionary trend. Gray CRB symbols denote samples exhibiting cumulate characteristics. Sources as in Fig. 3.

Eu (e.g., Defant and Drummond, 1990; Kay, 1978; Mamani et al., 2010). High Sr/Y (Sr/Y > 40) and/or La/Yb (La/Yb > 20) rocks, loosely termed "adakites," are often interpreted to reflect melting of a garnet-rich and plagioclase-absent (i.e., high-pressure) residue, originally thought to reflect slab melting, but more recently interpreted to reflect a pyroxene-rich and garnet-rich residue (Defant and Drummond, 1990; Gao et al., 2012; Moyen, 2009). Fig. 7 shows that all CRB samples except one have non-adakitic signatures, with average Sr/Y and La/Yb of 21 and 8, respectively. Group 2 samples show slightly higher La/Sm than Group 1 (~3.5 versus ~2.2), likely due to feldspar fractionation. Both groups have low Sm/Yb, ranging from 0.7 to 5.1. The degree of Eu anomaly [$Eu/Eu^* = Eu_N/(½{}^*Sm_N + Tb_N)$ (N denotes chondrite-normalized, Sun and McDonough, 1989)] does not appear to vary significantly with silica, with values ranging from 0.5 to 1.4 (Fig. 7).

4.5. Sr and Nd isotope geochemistry

Sr and Nd isotopic data are given in Table 3 for all sample groups except 1C, which was not analyzed, and includes results from metamorphic framework rocks, late-stage pegmatitic dikes, and hornblende and clinopyroxene separates from small Salinian mafic and ultramafic bodies. Group 1 and 2 samples define two distinct and enriched arrays in isotope plots (Fig. 8). Group 2 orthogneisses show elevated Sr_i from 0.7080 to 0.7092 at ε_{Nd} values of −0.7 to −5.9. Group 1 intrusives extend to higher ε_{Nd} (+1.4 to −3.0) and lower Sr_i (0.7061 to 0.7089).

The Nd and Sr isotopic values for framework metamorphic assemblages and pegmatite dikes span a wide range. Quartzites and quartzofeldspathic gneisses have $Sr_i > 0.708$ and $\varepsilon_{Nd} < -8$, consistent with derivation from old continental lithosphere. These values are similar to those of late-stage pegmatitic dikes in the area, suggesting a possible melting link between these lithologies. A sample of marble also has high Sr_i (0.709) at extremely low ε_{Nd} (−15.3), consistent with derivation from a Paleozoic miogeoclinal source.

Isotopic values from Salinian mafic and ultramafic bodies vary over a wide range from location to location. The tectonically emplaced and likely related (Bush, 1981) Chews Ridge and Pine Ridge bodies show extremely enriched, and likely altered by metasomatism, isotopic values ($Sr_i = 0.7161$ and 0.7085, and $\varepsilon_{Nd} = -9.5$ and +4.5, respectively). The igneous textured Escondido body yields Sr and Nd isotope ratios (Sr_i of ~0.7077 and $\varepsilon_{Nd} < -3.5$) that plot along the same trend as the CRB, suggesting a possible petrogenetic relationship and further implying that the Escondido body is an intrusion of enriched lithospheric upper mantle-derived melts.

A comparison of Salinian intrusives and the Escondido complex with other Cretaceous plutons of the California arc (Fig. 8) shows that Sr and Nd isotope ratios in the former are slightly shifted toward higher Sr_i at a

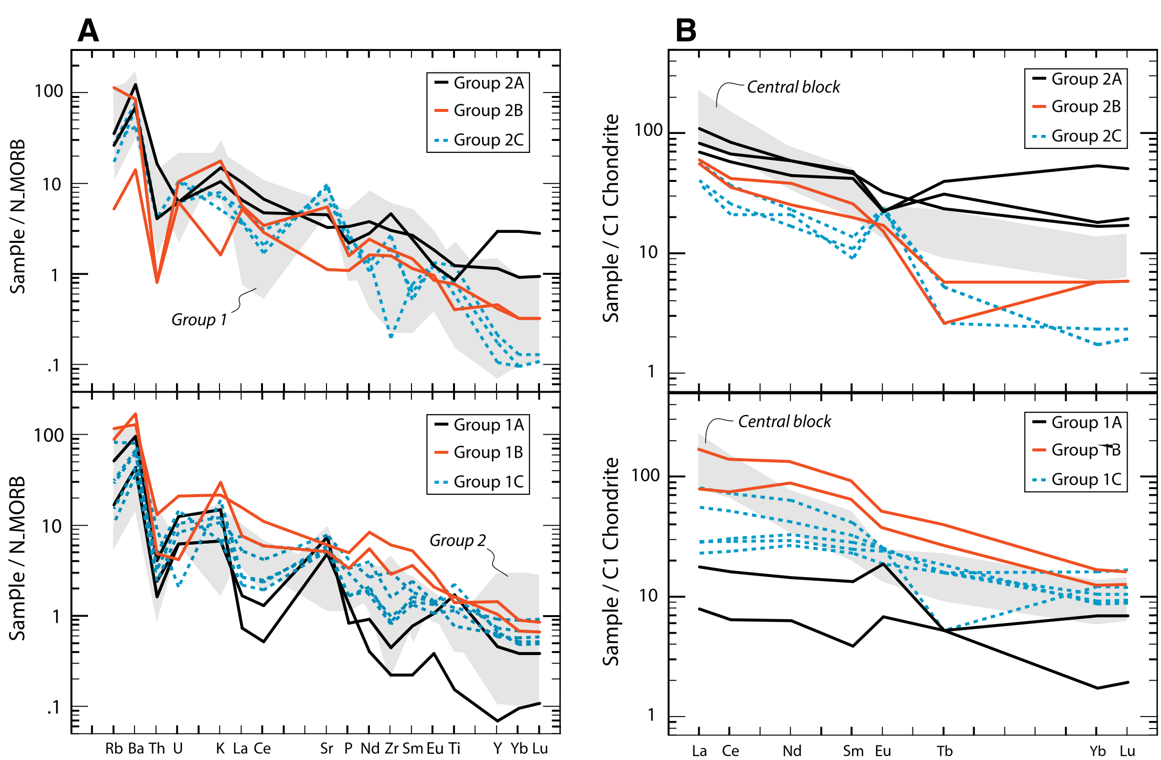

Fig. 5. N-MORB–normalized trace element (A) and chondrite-normalized REE (B) diagrams comparing sample groups of the CRB and the Central block (Ross, 1979, 1982). N-MORB and Chondrite values from Sun and McDonough (1989).

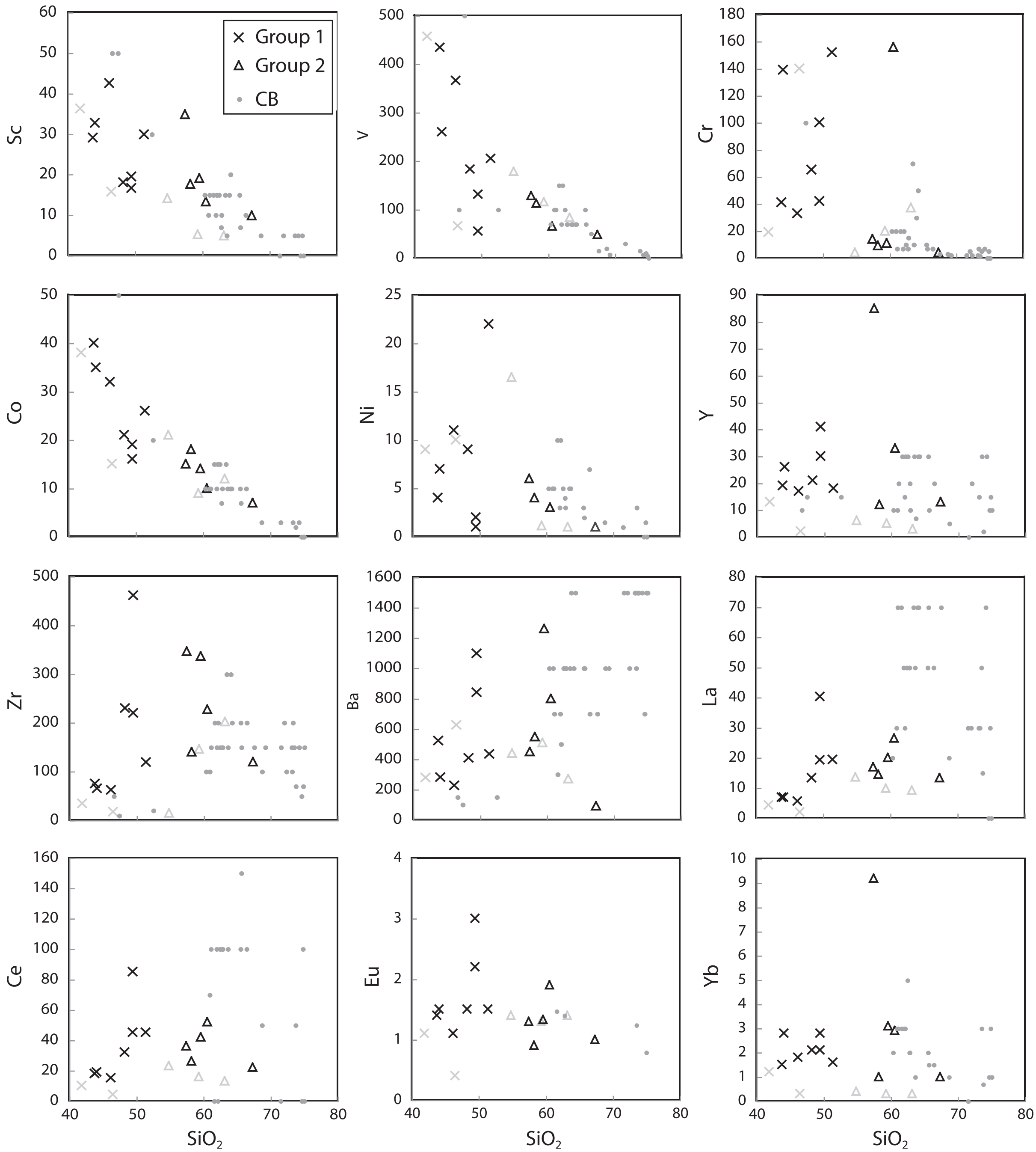

Fig. 6. Trace element variation diagrams for Group 1 and Group 2 samples of the CRB (Ross, 1979; this study) and the Central block (CB; Ross, 1972, 1979, 1982). Gray CRB symbols denote samples exhibiting cumulate characteristics.

given ε_{Nd}, exhibiting a trend similar to granitoids of the Mojave Desert (Miller et al., 1996) and conglomerate clasts of the Gualala basin (Schott et al., 2004).

5. Discussion

5.1. The Coast Ridge Belt — a titled exposure through an arc section

Geochemical and petrologic results presented here reveal several similarities between intrusive suites of the Salinian arc. First, well-defined linear variations of major elements, trace elements, and trace element ratios with silica show significant overlap for samples from both Groups 1 and 2 of the CRB and from the Central block (Figs. 2, 3, and 5). Furthermore, both groups of the CRB and samples from the Central block are metaluminous to mildly peraluminous, generally belong to the calc-alkaline series, exhibit weakly to moderately fractionated REE patterns, show small Eu anomalies, and have $Sr_i > 0.7061$ and $\varepsilon_{Nd} < +1.2$ (James, 1992; Kistler and Champion, 2001; Mattinson, 1978, 1990; Ross, 1982, this study). These data corroborate earlier field and geochronologic evidence (Kidder et al., 2003) that mafic (Group 1) and felsic (Group 2) magmas of the CRB are petrogenetically related. Geochemical data also support the interpretation that mafic arc magmas of the CRB and differentiated bodies of Central block were extracted from a similar source.

In the sections that follow, we evaluate the depth of magmagenesis and the relative importance of crystal fractionation, magma mixing, and

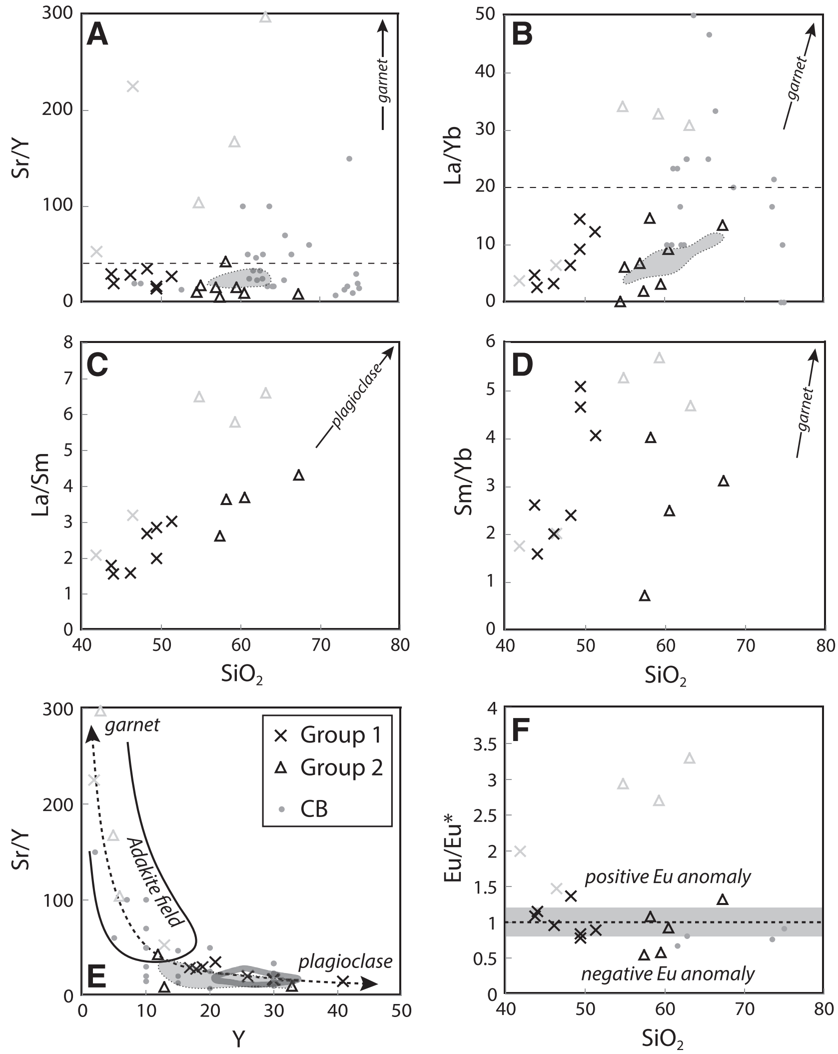

Fig. 7. Plot of Sr/Y (A), La/Yb (B), La/Sm (C), and Sm/Yb (D) versus wt.% SiO_2, Sr/Y versus Y (E), and Eu/Eu* versus wt.% SiO_2 (F) for Group 1 and Group 2 samples of the CRB (Ross, 1979; this study) and the Central block (CB; Ross, 1972, 1979, 1982). Adakite field in (E) from Defant and Drummond (1990). Dashed lines in (A) and (B) show cutoff values above which adakitic samples would plot. Dashed line in (E) represents trend expected for garnet- versus plagioclase-rich source. Europium anomaly (Eu/Eu*) in (F) denotes Eu divided by (Sm + Tb)/2. Eu/Eu* = 1.0 shown as dashed line and 20% uncertainty (Girardi et al., 2012) of calculated Eu/Eu* values shown as gray envelope. Gray CRB symbols denote samples exhibiting cumulate characteristics. Gray shaded fields with dotted outlines in A, B, and E show range of values in the southern Sierra Nevada batholith (Ross, 1989). Thick gray outlined field in (E) shows field of partial melts of amphibole-bearing, garnet-absent residues (Holland et al., 2013; Ratajeski et al., 2005).

partial melting processes in the petrogenesis of the CRB and compare our findings to other arc segments in the North American Cordillera.

5.2. Residual mineralogy and depth of melting

Several geochemical parameters suggest that the CRB resulted from melts in equilibrium with a plagioclase-stable and garnet-poor (or absent) residual (restite or cumulate) assemblage. First, several non-cumulate samples show negative Eu anomalies, suggesting the presence of plagioclase in the source. Second, samples from the CRB lack a "garnet signature" characterized by high Sr/Y, La/Yb, and Sm/Yb, and show an increase in La/Sm with silica, most likely due to plagioclase fractionation (Fig. 7). Positive correlations between SiO_2 and the LREE La to Sm and the lack of variability between SiO_2 and heavier REE further argue for plagioclase and against garnet as major phases in the site of magma generation.

Three geochemical relations suggest the presence of amphibole in the low silica residual assemblage. First, all Group 1 and several Group 2 plutons of the CRB have low Y contents (<20 ppm) at low Sr/Y (<40). A source containing plagioclase and amphibole and lacking garnet provides an attractive explanation for melts with low Y and low Sr/Y, given plagioclase/melt and amphibole/melt partition coefficients for Y (0.005 and 1.56, respectively) and Sr (1.84 and 0.72, respectively; Foley, 2008). Experimental melts including plagioclase and amphibole and lacking garnet in the source (Ratajeski et al., 2005) provide a good match for plutons of the CRB (Fig. 7E). Second, rare-earth element patterns for CRB plutons show enrichment in LILE, depletion of HREE relative to LREE, and concave upward MREE depletion. These features are consistent with partial melting in equilibrium with residues containing appreciable amphibole, which preferentially incorporates MREE. Finally, K_2O values decrease slightly with SiO_2 (Fig. 3A) and low K/Rb values (averaging ~375) do not vary significantly with SiO2 (Fig. 9). These observations require that the residual mineral assemblage is K-rich with a larger bulk distribution coefficient for K than for Rb.

Experimental (e.g., Green and Ringwood, 1967; Ito and Kennedy, 1971; Rapp and Watson, 1995; Wolf and Wyllie, 1994; Wyllie and Wolf, 1993), thermodynamic (e.g., DePaoli et al., 2012; Ducea, 2002), and thermobarometric (e.g., Ducea and Saleeby, 1996; O'Brien and Rötzler, 2003) studies indicate that the appearance of garnet and the breakdown of plagioclase are critically dependent on pressure, temperature, and bulk composition. For the average composition of the Sierra

Table 3
Sr and Nd isotope data.

Sample	$^{87}Rb/^{86}Sr$	$^{87}Sr/^{86}Sr(0)$	$^{87}Sr/^{86}Sr(90)$	$^{147}Sm/^{144}Nd$	$^{143}Nd/^{144}Nd(0)$	$\varepsilon_{Nd}(90)$
Group 2A						
1				0.13402	0.512346	−4.7
2	0.19415	0.708835	0.708587			
Group 2B						
3	0.38173	0.709676	0.709188	0.13402	0.512288	−5.9
4	0.08458	0.708100	0.707992	0.13402	0.512551	−0.7
Group 1A						
8	0.04173	0.707489	0.707436	0.184553	0.512538	−1.6
9	0.18886	0.708121	0.707880			
Group 1B						
10	0.345	0.707881	0.707440	0.136437	0.512478	−2.2
11	0.31046	0.706482	0.706085	0.142707	0.512663	1.4
Group 1C						
12	0.03687	0.707232	0.707185	0.171519	0.512459	−3.0
13	0.06741	0.709002	0.708916			
14	0.05062	0.706667	0.706602	0.17154	0.512642	0.6
16	0.10845	0.707299	0.707160	0.130271	0.512484	−2.0
Non-deformed (late) intrusive rocks						
17	0.0838	0.710734	0.710627	0.124986	0.512182	−7.8
18				0.124986	0.512091	−9.6
Framework metasedimentary rocks						
19	0.19415	0.708835	0.708587			
21	0.66057	0.712832	0.711988	0.121998	0.512156	−8.3
22	0.05025	0.709024	0.708960	0.112928	0.511791	−15.3
Small ultramafic–mafic bodies[a]						
23H	0.047	0.707785	0.707725	0.183	0.512401	−4.2
23C	0.0467	0.707760	0.707700	0.183	0.512438	−3.5
24H	0.0108	0.707622	0.707608	0.183	0.512433	−3.6
25C	0.0177	0.716117	0.716094	0.099032	0.512082	−9.5
26C	0.0452	0.708493	0.708435	0.170447	0.512838	4.5

Estimated analytical $\pm 2\sigma$ uncertainties: $^{87}Rb/^{86}Sr = 0.55\%$, $^{87}Sr/^{86}Sr = 0.0014\%$, $^{147}Sm/^{144}Nd = 0.8\%$, and $^{143}Nd/^{144}Nd = 0.002\%$.
[a] C, clinopyroxene separate; H, hornblende separate.

Nevada batholith, this transition from garnet-in to plagioclase-out takes place over a depth range of ~40 to 60 km at temperatures above 800 °C. Therefore, based on geochemical evidence suggesting the presence of plagioclase and absence of appreciable garnet in the source of the CRB, it is likely that these assemblages underwent magmatic processing at depths shallower than ~40 km. These results imply that the CRB was emplaced into crust that had not experienced significant crustal thickening due to tectonic shortening or magmatic additions when compared to other segments of the California arc.

Peak metamorphic conditions of ~7 to 8 kbar and ~700 to 800 °C were achieved in the CRB during and immediately following igneous construction (Ducea et al., 2003a; Hansen and Stuk, 1993; Kidder et al., 2003), requiring that the depth of magmagenesis exceeded ~25 km. Therefore, the depth of melting for the CRB is bracketed by geochemical and thermobarometric data to between ~40 and 25 km, indicating that CRB magmas did not ascend more than a few kilometers before stalling and crystallizing. Furthermore, the calculated melting paleodepth interval is consistent with our previous assertion (Ducea et al., 2003a; Kidder et al., 2003) that the CRB represents a window into the root zone for batholith-scale intrusions, locally exposed at shallower levels in the Central block to the east of the CRB (John, 1981; Kistler and Champion, 2001; Wiebe, 1966, 1970).

Shallow depths of melting (<40 km) are also documented in the west-central Sierra Nevada batholith (Holland et al., 2013), the western Peninsular Ranges batholith (Gromet and Silver, 1987), the Chilliwack batholith (North Cascades; Tepper et al., 1993) and can be inferred for deep (>30 km; Pickett and Saleeby, 1993) exposures of the southwestern Sierra Nevada based on Sr/Y and La/Yb values of <35 and <16, respectively (Ross, 1989). The inferred depth of magmagenesis

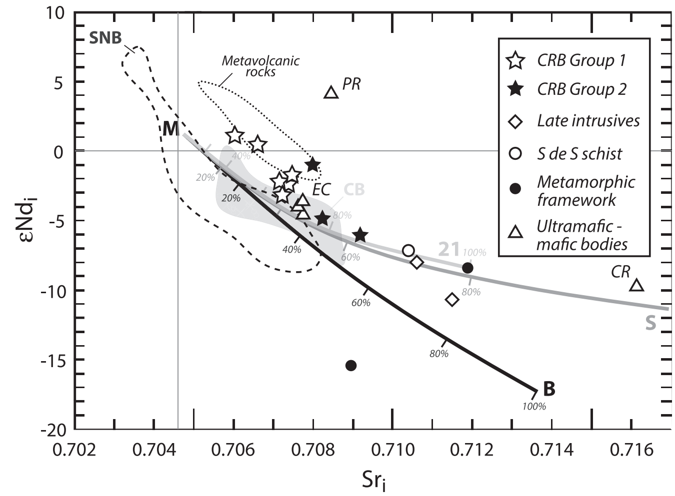

Fig. 8. Sr and Nd isotopic compositions for Coast Ridge Belt (CRB) samples compared to Cretaceous plutons of the Sierra Nevada batholith and the Central block and metavolcanic rocks of the Sierra Nevada batholith. Intersecting axes are “bulk earth” values. Epsilon values and Sr ratios are initial values for granitoids; values for metamorphic framework and ultramafic-mafic bodies are age-corrected for 90 Ma. Tick marks on mixing curves denote percent supracrustal component. Average Sierran metasedimentary framework “S” ($^{143}Nd/^{144}Nd = 0.51192$, $Sr_i = 0.71759$, Nd = 24 ppm, Sr = 182 ppm) value averaged from DePaolo (1981) and Pickett and Saleeby (1994). Mantle “M” ($^{143}Nd/^{144}Nd = 0.51256$, $Sr_i = 0.7047$, Nd = 24 ppm, Sr = 555 ppm) value from Kistler et al. (1986). Mojave lower crustal basement “B” ($^{143}Nd/^{144}Nd = 0.51163$, $Sr_i = 0.7136$, Nd = 24 ppm, Sr = 412 ppm) value from Miller et al. (2000). Sample 21 metamorphic rock labeled as “21.” Pine Ridge (PR), Chews Ridge (CR), and Escondido complex (EC) ultramafic-mafic bodies are labeled. Other abbreviations: CB, Central block; SNB, Sierra Nevada batholith; S de S, Sierra de Salinas (Mattinson, 1990).

for the CRB is shallower than >40 km paleodepths inferred from the central and eastern Sierra Nevada (Cecil et al., 2012; Ducea, 2001) and Peninsular Ranges (Gromet and Silver, 1987) batholiths, the Idaho (Gaschnig et al., 2011) and Coast Mountains (Girardi et al., 2012) batholiths, and tonalitic plutons of the Cascades core (Miller et al., 2009).

5.3. Isotopic constraints on magma mixing and alteration

Initial $^{87}Sr/^{86}Sr$ (0.7061 to 0.7092) and ε_{Nd} (+1.4 to −5.9) values of the CRB and the majority of the Central block (Kistler and Champion, 2001; Mattinson, 1978, 1990; this study) require significant involvement of ancient continental lithospheric material in the magmatic source. These isotopic data define a mixing trend bracketed by low Sr_i–high ε_{Nd} and high Sr_i–low ε_{Nd} end-members (Fig. 8), with Group 2 values extending to higher Sr_i and lower ε_{Nd} than Group 1. A common explanation for similar isotopic trends in Cordilleran batholiths is that they represent mixtures of primitive mantle melts and supracrustal end-member(s) (e.g., DePaolo, 1981; Gaschnig et al., 2011; Girardi

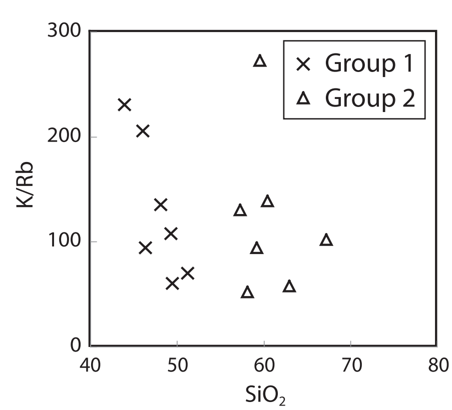

Fig. 9. Plot of K/Rb versus wt.% SiO_2 for CRB rocks.

et al., 2012; Lackey et al., 2005, 2008; Pickett and Saleeby, 1994). The heterogeneity of Salinian plutons (e.g., Compton, 1966; Kidder et al., 2003) and the presence of continuous linear trends of major elements, trace elements, and trace element ratios with silica point to a mixing origin for these rocks.

To determine if mixing of various crust and mantle reservoirs can account for the correlation between ε_{Nd} and Sr_i, bulk mixing calculations were done (Fig. 8). An ancient North American mantle lithosphere (Kistler et al., 1986) reservoir was selected as the most likely low Sr_i–high ε_{Nd} end member since the isotopic baselines of mafic plutons within the CRB, western Mojave, and the southern Sierra Nevada batholith are not consistent with a depleted mantle source (Pickett and Saleeby, 1994; Saleeby, 2011). Furthermore, the Escondido complex, an ultramafic body likely derived from partial melting of lithospheric upper mantle, provides evidence of enriched sub-batholithic mantle in the Salinian arc. Crustal components, including representative samples and averages of metasedimentary rocks (DePaolo, 1981; Pickett and Saleeby, 1994; Zeng et al., 2005) and crystalline basement of the Mojave Desert (Miller et al., 2000), were adopted as potential high Sr_i–low ε_{Nd} end-members.

Mixing trends are shown in Fig. 8. In general, simple mixing models between mantle and crustal end members reproduce the observed isotopic values. Data from the CRB lie in closer proximity to curves involving metasedimentary as opposed to basement end members. This observation strongly suggests that CRB magmas were derived from a source containing a higher proportion of metasedimentary material than the bulk of the California arc (Ducea, 2001). Oxygen isotope values of +8.5 to +9.8‰ relative to SMOW in the Salinian block *sensu lato* (Kistler and Champion, 2001) are consistent with a significant sedimentary component in the source of CRB plutons.

Mixing curves (Fig. 8) suggest that the magmatic source for the CRB contained at least 10–40% and 30–60% average Sierran metasedimentary material for Group 1 and Group 2 assemblages, respectively. Isotopic compositions of postkinematic leucrogranite dikes require higher proportions, approaching pure melts of average metasedimentary material in the source. The interpretation of a large metasedimentary input into magmas of the CRB is also consistent with an evolved Pb signature in Salinian central belt plutons with well-defined arrays in $^{208}Pb/^{204}Pb$–$^{206}Pb/^{204}Pb$ and $^{207}Pb/^{204}Pb$–$^{206}Pb/^{204}Pb$ spaces, overlapping trends seen in the western Mojave Desert and Gualala Basin (Mattinson, 1990; Schott et al., 2004) and highly radiogenic "Area II-type Pb" of Zartman (1974). The Salinian Pb signature is distinct from Late Cretaceous granitoids of the eastern Mojave Desert and central Sierra Nevada batholith (Chen and Tilton, 1991; Mattinson, 1990; Wooden et al., 1988). Furthermore, inherited zircon grains (Kidder et al., 2003; Kistler and Champion, 2001; Mattinson, 1978) in CRB plutons show similar pre-Mesozoic zircon age spectra to those of the Sur Series (Barbeau et al., 2005), suggesting significant assimilation of framework rocks during emplacement of the CRB.

One additional component and/or post-emplacement alteration is/are required to explain elevated Sr_i at a given ε_{Nd} with respect to modeled mixing curves and to the isotopic field of the Sierra Nevada batholith (Fig. 8). Similar enrichments in Sr_i at a given ε_{Nd} are also exhibited in granitoids from the Salinian Central block, western Mojave Desert, Gualala Basin, and southern Sierra Nevada (Kistler and Champion, 2001; Mattinson, 1990; Miller et al., 1996; Pickett and Saleeby, 1994; Schott et al., 2004). One explanation for the isotopic signature of the CRB is that significant amounts of downgoing trench sediments and/or oceanic crust, perhaps altered by seawater (e.g., McCulloch et al., 1980), were present within the magmatic source (e.g., Chapman et al., 2013). Alternatively, a groundwater alteration process is also consistent with the data, as meteoric water also has low concentrations in REE compared to Sr.

The distinct isotopic values from the southern Sierra Nevada–Mojave–Salinia corridor (Fig. 1 inset) strongly suggest that they crystallized from magmas derived from different source components than those of the greater Sierra Nevada batholith. Kistler (1990) suggested, based primarily on elevated Sr_i and $\delta^{18}O$ values in plutons, that the pre-intrusive basement of this western Mojave consisted of abyssal and metasedimentary rocks, termed "Panthalassan lithosphere," and that a distinct "North American lithosphere" containing Proterozoic crystalline basement was present to the east. Isotopic relations from plutons of the southern Sierra Nevada–Mojave–Salinia corridor are qualitatively most consistent with assimilation of high $\delta^{18}O$, Sr_i, and $^{208}Pb/^{204}Pb$ and low ε_{Nd} material, a fingerprint most likely acquired from Panthalassan sediments.

In summary, mixing of continental (North American) lithospheric upper mantle- and metasedimentary framework-derived melts (sourced from Panthalassan basement and cover) provides the simplest explanation for the isotopic values measured on igneous rocks of the CRB, although a cryptic third sea/groundwater and/or trench material component may be required as well.

5.4. Origin of Coast Ridge Belt plutons

The CRB was constructed by compositionally diverse magmatic additions over a brief time interval, between ca. 93 and 80 Ma (Kidder et al., 2003), and was extinguished as abruptly as it began, presumably due to mechanical delamination of the Salinian lithospheric mantle and lower crustal root associated with shallowing of the Farallon plate (e.g., Saleeby, 2003). The CRB represents a rare window into a lower crustal arc zone for batholith-forming intrusions, wherein metasedimentary framework rocks were assimilated by mantle-derived melts, thereby producing silicic hybrid magmas. This origin is supported by the covariation between ε_{Nd} and Sr_i values, which require mixing of a significant amount of supracrustal material of the former passive North American margin with continental lithospheric mantle-derived melts. The Sur Series and deeper crustal equivalents of the Panthalassa realm are the most likely supracrustal contributors.

Melting experiments are consistent with a hybrid origin for plutons of the CRB. Experimental reaction of basaltic melts with metasedimentary rocks at low pressure ($P < 10$ kbar) produces compositions overlapping those of the CRB (Fig. 10; Patino Douce, 1999). Metaluminous to weakly peraluminous alumina saturation indices (0.4 to 1.1) further suggest, based on the discrimination scheme of Patino Douce (1999), that the compositions of CRB plutons are best explained by mafic additions of ~50% (for Group 1) and at least 50% (for Group 2). This observation is consistent with our ε_{Nd}–Sr_i bulk mixing calculations suggesting additions of between 10 to 60% average metasedimentary material for CRB plutons. Central block plutons represent more pure crustal melts than those of the CRB, with compositions similar to experimental dehydration melts of various metasediments (Patino Douce, 1999).

Underplating of melts derived from evolved lithospheric mantle provides a viable mechanism explaining geochemical (e.g., continuous elemental and isotopic trends; Figs. 3,4, 6, 7, 8, 9, and 11) and field evidence for crustal melting (e.g., migmatitic textures) in the CRB (Hansen and Harlov, 2009; Hansen and Stuk, 1993; Kidder et al., 2003; this study). We suggest that the thermal pulse provided by basaltic underplating (e.g., Tepper et al., 1993) to the base of the crust led to an initial episode of metasediment assimilation by Group 1 plutons, followed soon thereafter by remelting of these intrusions to produce more silicic Group 2 magmas and migmatitic textures in Group 1 rocks. By this model, the apparent higher proportion of metasedimentary material in Group 2 plutons resulted through anatexis of Group 1 plutons and/or previously unmelted Sur Series assemblages. However, our results cannot rule out the possibility that Group 2 plutons crystallized from an original melt.

5.5. Supracrustal input into an arc root zone

Field, petrographic, geochemical, and isotopic evidence presented here strongly suggest that plutonic assemblages of the CRB represent

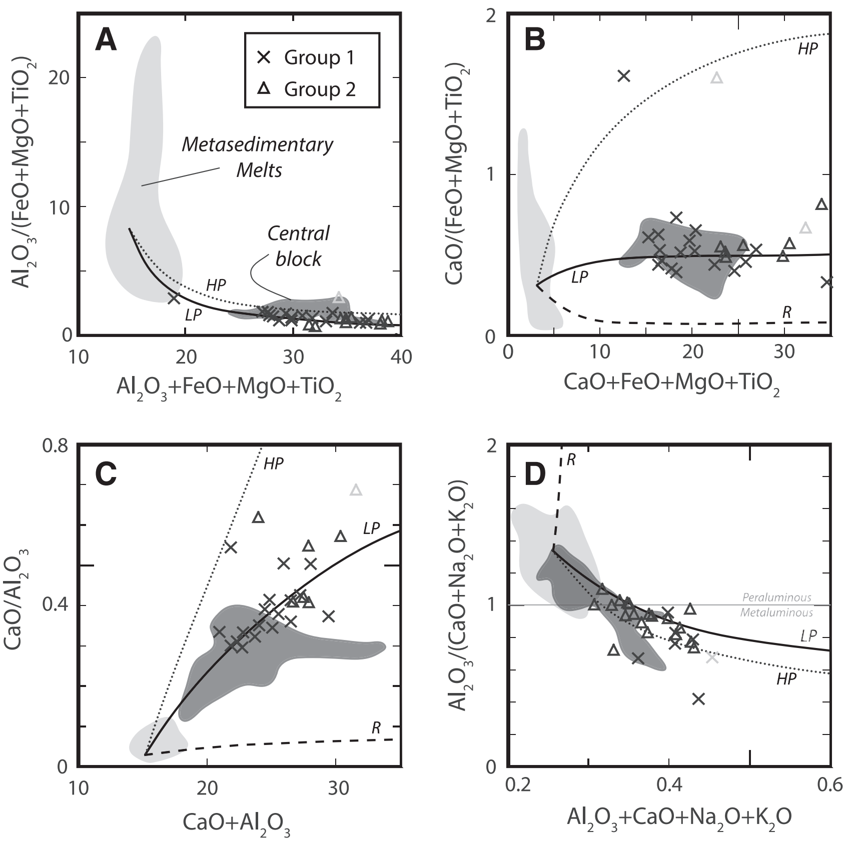

Fig. 10. Comparison of major element compositions of the CRB and Central block plutons with experimental melts (Patino Douce, 1999). Curves represent high-pressure (HP; >12 kbar) and low-pressure (LP; <5 kbar) melt and restite (R) compositions produced through hybridization of basaltic and metasedimentary melts. Note that CRB and Central block plutons generally plot along low-pressure hybrid curves. Units in (A), (B), and (C) are wt.% oxide. Units in (D) are molar $Al_2O_3/(CaO + Na_2O + K_2O)$ versus molar $Al_2O_3 + CaO + Na_2O + K_2O$. Note in (D) that peraluminous low pressure melts are possible with up to ~50% basaltic input (Patino Douce, 1999).

hybrid magmas produced through interaction of basaltic underplate with partially melted metasedimentary framework rocks at relatively shallow levels (25–40 km). Emplacement of the Salinian arc occurred at the peak of an episode of voluminous arc magmatism that affected several Cordilleran arc segments (Coleman and Glazner, 1998; DeCelles et al., 2009; Ducea, 2001). These high-flux events often correspond with increased input of upper plate material in the source compared to periods of low magmatic flux (Ducea and Barton, 2007). Our results permit speculation about the most likely mechanism(s) by which supracrustal material was displaced downward into the magma source of the CRB.

This study shows that metasedimentary assemblages of the miogeocline, including the Sur Series, were important supracrustal contaminants into the Salinian arc and input of trench sediments and/or altered oceanic crust was relatively minor (Fig. 11). We speculate that displacement of miogeoclinal assemblages into the root zone of the Salinian arc was achieved within a crustal-scale convection system and that retroarc thrusting did not play a major role, for the following

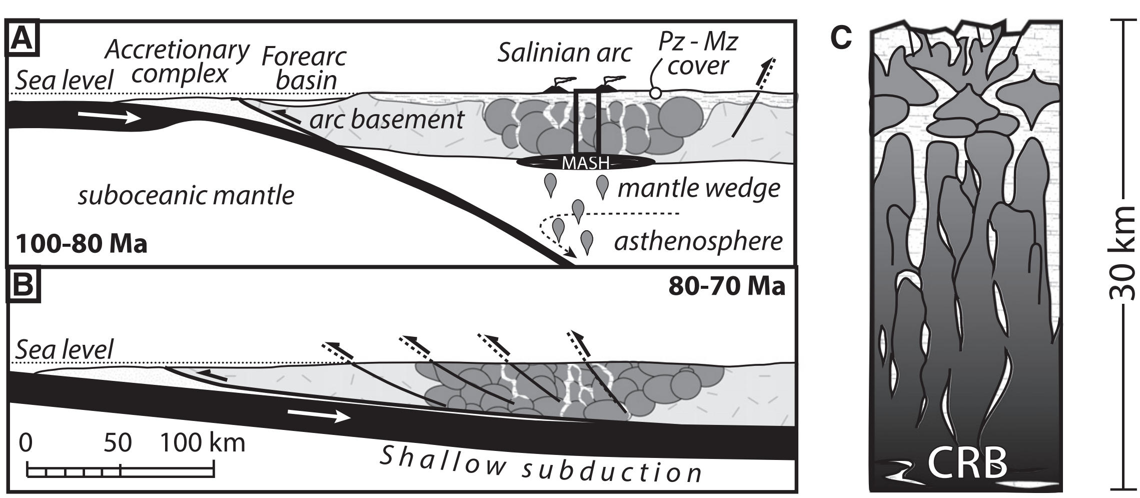

Fig. 11. Generalized cross-section model for the Salinian arc. Note downward transport of Paleozoic–Mesozoic host rocks in panels (A), enlarged in (C). (A) Ca. 100–80 Ma subduction of Farallon plate beneath North America prior to shallow subduction, downward host rock transport, and ignition of the Salinian arc, (B) ca. 80–70 Ma flat subduction, mechanical lithospheric mantle and lowermost crust removal, arc shutoff, and underplating of the schist of Sierra de Salinas, (C) enlarged view of (A), showing location of Coast Ridge Belt (CRB).

reasons: 1) field evidence for the deflection of foliation trajectories from subvertical to subhorizontal with increasing paleodepth (Kidder et al., 2003) is more consistent with intra-arc downflow versus ductile thrusting and 2) there is little evidence for major Late Cretaceous retroarc thrusting in the pre-San Andreas position of Salinia (e.g., DeCelles, 2004; DeCelles and Coogan, 2006; Fig. 1 inset). A detailed structural and geochronologic study of metavolcanic assemblages within the CRB, which imply eruption at the surface and subsequent displacement to 20–30 km paleodepths, may permit evaluation of this hypothesis. However, to our knowledge, metavolcanic rocks are not recognized in Salinia except within Central block plutons at Garrapata Beach (D. Barbeau, unpublished data; Fig. 1).

Downward displacement of supracrustal assemblages during plutonism has been invoked to explain the incorporation of supracrustal assemblages in several arc segments in North and South America (Babeyko et al., 2002; Miller et al., 2009; Paterson and Farris, 2008; Saleeby, 1990). The widespread recognition of evidence supporting downward host rock transport suggests that it is an important process controlling crustal growth and the formation of arc roots, such as the CRB.

6. Conclusions

We report new major and trace element concentrations as well as Sr and Nd isotopic analyses from representative rocks of the CRB, an exposure of a lower crustal batholithic root in the California arc. The entire igneous section was built between 93 and 81 Ma, and intruded supracrustal framework rocks of the Sur Series. REE patterns in igneous and metaigneous rocks of the CRB suggest that they are sourced deeper than the ~25 km paleodepths represented by the exposed section (Hansen and Stuk, 1993; Kidder et al., 2003), but probably not below 40–50 km. Group 2 tonalites and Group 1 gabbroids of the CRB are predominantly calc-alkaline, one third of which exhibit cumulate characteristics, and all show enriched isotopic compositions ($Sr_i = 0.7061$ to 0.7092 and $\varepsilon_{Nd} = +1.4$ to -5.9). Mafic to ultramafic intrusions of the Escondido complex yield enriched Sr and Nd isotope ratios that plot along the same trend as the CRB, suggesting that the Escondido body is an intrusion of enriched lithospheric upper mantle-derived melts. We suggest that underplating of basaltic melts derived from evolved lithospheric mantle provides the most satisfactory mechanism explaining geochemical and field evidence for melting and assimilation of the metasedimentary framework. This mechanism is especially efficient during the early periods of subduction-related arc magmatism, when mantle-derived melts are emplaced into a melt-fertile thick accumulation of passive margin-type sediments (Otamendi et al., 2009; Wetmore and Ducea, 2011). Miogeoclinal assemblages most likely flowed downward into the root zone of the Salinian arc within a crustal-scale convection system.

Acknowledgements

This research was supported by NSF EAR grants 1019525 (Ducea) and 1250070 (Chapman) and UEFISCDI grant PN-II-ID-PCE-2011-3-0217. The article benefitted from discussions with P. Asimow, P. DeCelles, J. Eiler, S. Paterson, and J. Saleeby, thoughtful and constructive comments by Robert Miller and an anonymous reviewer, and editorial handling by Nelson Eby. Beth Duschatko performed some of the isotopic measurements as part of her undergraduate work at the University of Arizona.

References

Babeyko, A.Yu., Sobolev, S.V., Trumbull, R.B., Oncken, O., Lavier, L.L., 2002. Numerical models of crustal scale convection and partial melting beneath the Altiplano–Puna Plateau. Earth and Planetary Science Letters 199, 373–388.

Barbeau Jr., D.L., Ducea, M.N., Gehrels, G.E., Kidder, S., Wetmore, P.H., Saleeby, J.B., 2005. U–Pb detrital-zircon geochronology of northern Salinian basement and cover rocks. Geological Society of America Bulletin 117, 466–481.

Barker, F., Arth, J.G., 1984. Preliminary results, Central Gneiss Complex of the Coast Range Batholith, southeastern Alaska; the roots of a high-K, calc-alkaline arc? Physics of the Earth and Planetary Interiors 35, 191–198.

Barth, A.P., May, D.J., 1992. Mineralogy and pressure–temperature–time path of Cretaceous granulite gneisses, south-eastern San Gabriel Mountains, southern California. Journal of Metamorphic Geology 10, 529–544.

Barth, A.P., Wooden, J.L., Grove, M., Jacobson, C.E., Pedrick, J.N., 2003. U–Pb zircon geochronology of rocks in the Salinas Valley region of California: a reevaluation of the crustal structure and origin of the Salinian Block. Geology 31 (6), 517–520 (10.1130/0091-7613(2003)031<0517:UZGORI>2.0.CO;2).

Behn, M.D., Kelemen, P.B., Hirth, G., Hacker, B.R., Massonne, H.-J., 2011. Diapirs as the source of the sediment signature in arc lavas. Nature Geoscience 4, 641–646. http://dx.doi.org/10.1038/ngeo1214.

Bush, R.N., 1981. Small Salinian Ultramafic Bodies Near Jamesburg, California. (M.S. thesis) Stanford University (123 pp.).

Cecil, M.R., Rotberg, G.L., Ducea, M.N., Saleeby, J.B., Gehrels, G.E., 2012. Magmatic growth and batholithic root development in the northern Sierra Nevada, California. Geosphere 8, 592–606. http://dx.doi.org/10.1130/GES00729.1.

Chapman, A.D., Kidder, S., Saleeby, J.B., Ducea, M.N., 2010. Role of extrusion of the Rand and Sierra de Salinas schists in Late Cretaceous extension and rotation of the southern Sierra Nevada and vicinity. Tectonics 29. http://dx.doi.org/10.1029/2009TC002597.

Chapman, A.D., Luffi, P., Saleeby, J., Petersen, S., 2011. Metamorphic evolution, partial melting, and rapid exhumation above an ancient flat slab: insights from the San Emigdio Schist, southern California. Journal of Metamorphic Geology 29, 601–626. http://dx.doi.org/10.1111/j.1525-1314.2011.00932.x.

Chapman, A.D., Saleeby, J.B., Wood, D.J., Piasecki, A., Farley, K.A., Kidder, S., Ducea, M.N., 2012. Late Cretaceous gravitational collapse of the southern Sierra Nevada batholith, California. Geosphere 8, 314–341. http://dx.doi.org/10.1130/GES00740.1.

Chapman, A.D., Saleeby, J.B., Eiler, J.M., 2013. Slab flattening trigger for isotopic disturbance and magmatic flare-up in the southernmost Sierra Nevada batholith, California. Geology 41 (9), 1007–1010. http://dx.doi.org/10.1130/G34445.1.

Chen, J.H., Tilton, G.R., 1991. Applications of lead and strontium isotopic relationships to the petrogenesis of granitoid rocks, central Sierra Nevada batholith, California. Geological Society of America Bulletin 103, 439–447.

Chin, E.J., Lee, C.-T.A., Tollstrup, D.L., Xie, L.-W., Wimpenny, J.B., Yin, Q.-Z., 2013. On the origin of hot metasedimentary quartzites in the lower crust. Earth and Planetary Science Letters 361, 120–133.

Christensen, N.I., Mooney, W.D., 1995. Seismic velocity structure and composition of the continental crust: a global view. Journal of Geophysical Research 100 (B7), 9761–9788.

Coleman, D.S., Glazner, A.F., 1998. The Sierra Crest magmatic event: rapid formation of juvenile crust during the Late Cretaceous in California. In: Ernst, W.G., Nelson, C.A. (Eds.), Integrated Earth and Environmental Evolution of the Southwestern United States: The Clarence A. Hall, Jr. Volume. Bellwether, Columbia, MD, pp. 253–272.

Compton, R.R., 1960. Charnockitic rocks of Santa Lucia Range, California. American Journal of Science 258, 609–636.

Compton, R.R., 1966. Granitic and metamorphic rocks of the Salinian block, California Coast Ranges. Bulletin California Division of Mines and Geology 90, 277–287.

DeCelles, P.G., 2004. Late Jurassic to Eocene evolution of the Cordilleran thrust belt and foreland basin system, western U.S.A. American Journal of Science 304, 105–168.

DeCelles, P.G., Coogan, J.C., 2006. Regional structure and kinematic history of the Sevier fold-and-thrust belt, central Utah. Geological Society of America Bulletin 118, 841–864. http://dx.doi.org/10.1130/B25759.1.

DeCelles, P., Ducea, M., Kapp, P., Zandt, G., 2009. Cyclicity in cordilleran orogenic systems. Nature Geoscience 2. http://dx.doi.org/10.1038/ngeo469.

Defant, M.J., Drummond, M.S., 1990. Derivation of some modern arc magmas by melting of young subducted lithosphere. Nature 347, 662–665.

DePaoli, M.C., Clarke, G.L., Daczko, N.R., 2012. Mineral equilibria modeling of the granulite–eclogite transition: effects of whole-rock composition on metamorphic facies type-assemblages. Journal of Petrology 53, 949–970. http://dx.doi.org/10.1093/petrology/egs004.

DePaolo, D.J., 1981. A neodymium and strontium isotopic study of the Mesozoic calc-alkaline granitic batholiths of the Sierra-Nevada and Peninsular Ranges, California. Journal of Geophysical Research 86, 470–488.

Dickinson, W.R., Ducea, M., Rosenberg, L.I., Greene, H.G., Graham, S.A., Clark, J.C., Weber, G.E., Kidder, S., Ernst, G.W., Brabb, E.E., 2005. Net dextral slip, Neogene San Gregorio–Hosgri fault zone, coastal California: geologic evidence and tectonic implications. Geological Society of America, Special Paper 391 (43 pp.).

Ducea, M., 2001. The California Arc; thick granitic batholiths, eclogitic residues, lithospheric-scale thrusting, and magmatic flare-ups. GSA Today 11, 4–10.

Ducea, M.N., 2002. Constraints on the bulk composition and root foundering rates of continental arcs; a California arc perspective. Journal of Geophysical Research 107. http://dx.doi.org/10.1029/2001JB000643.

Ducea, M.N., Barton, M.D., 2007. Igniting flare-up events in Cordilleran arcs. Geology 35, 1047–1050.

Ducea, M.N., Saleeby, J.B., 1996. Buoyancy sources for a large, unrooted mountain range, the Sierra Nevada, California; evidence from xenolith thermobarometry. Journal of Geophysical Research 101, 8229–8244.

Ducea, M.N., Kidder, S., Zandt, G., 2003a. Arc composition at mid-crustal depths; insights from the Coast Ridge Belt, Santa Lucia Mountains, California. Geophysical Research Letters 30. http://dx.doi.org/10.1029/2002GL016297.

Ducea, M.N., Ganguly, J., Rosenberg, E.J., Patchett, P.J., Cheng, W.J., Isachsen, C., 2003b. Sm–Nd dating of spatially controlled domains of garnet single crystals: a new method of

high-temperature thermochronology. Earth and Planetary Science Letters 213, 31–42. http://dx.doi.org/10.1016/S0012- 821X(03)00298-X.
Ducea, M.N., Kidder, S., Chelsey, J.T., Saleeby, J.B., 2009. Tectonic underplating of trench sediments beneath magmatic arcs, the central California example. International Geology Review 51, 1–26. http://dx.doi.org/10.1080/00206810802602767.
Foley, S., 2008. A trace element perspective on Archean crust formation and on the presence or absence of Archean subduction. Geological Society of America, Special Paper 440, 31–50.
Frost, B.R., Barnes, C.G., Collins, W.J., Arculus, R.J., Ellis, D.J., Frost, C.D., 2001. A geochemical classification for granitic rocks. Journal of Petrology 42, 2033–2048.
Gao, Y., Santosh, M., Hou, Z., Wei, R., Ma, G., Chen, Z., Wu, J., 2012. High Sr/Y magmas generated through crystal fractionation: evidence from Mesozoic volcanic rocks in the northern Taihang orogen, North China Craton. Gondwana Research 22, 152–168. http://dx.doi.org/10.1016/j.gr.2011.11.002.
Gaschnig, R.M., Vervoort, J.D., Lewis, R.S., Tikoff, B., 2011. Isotopic evolution of the Idaho Batholith and Challis intrusive province, Northern US Cordillera. Journal of Petrology 52, 2397–2429. http://dx.doi.org/10.1093/petrology/egr050.
Girardi, J.D., Patchett, P.J., Ducea, M.N., Gehrels, G.E., Cecil, M.R., Rusmore, M.E., Woodsworth, G.J., Pearson, D.M., Manthei, C., Wetmore, P., 2012. Elemental and Isotopic evidence for granitoid genesis from deep-seated sources in the Coast Mountains Batholith, British Columbia. Journal of Petrology 53, 1505–1536. http://dx.doi.org/10.1093/petrology/egs024.
Green, D.H., Ringwood, A.E., 1967. An experimental investigation of the gabbro-to-eclogite transformation and its petrological applications. Geochimica et Cosmochimica Acta 31, 767–833.
Gromet, L.P., Silver, L.T., 1987. REE variations across the Peninsular Ranges Batholith; implications for batholithic petrogenesis and crustal growth in magmatic arcs. Journal of Petrology 28, 75–125.
Hacker, B.R., Kelemen, P.B., Behn, M.D., 2011. Differentiation of the continental crust by relamination. Earth and Planetary Science Letters 307, 501–516.
Hall Jr., C.A., 1991. Geology of the Point Sur-Lopez Point region, Coast Ranges, California; a part of the Southern California Allochthon: Boulder, CO, United States. Geological Society of America, Special Paper 266, 1–40.
Hall, C.A., Saleeby, J., 2013. Salinia revisited: a crystalline nappe sequence lying above the Nacimiento fault and dispersed along the San Andreas fault system, central California. International Geology Review 55 (13), 1575–1615. http://dx.doi.org/10.1080/00206814.2013.825141.
Hansen, E.C., Harlov, D.E., 2009. Orthophosphate and biotite chemistry from orthopyroxene-bearing migmatites from California and South India: the role of a fluid-phase in the evolution of granulite-facies migmatites. Mineralogy and Petrology 95, 201–217.
Hansen, E., Stuk, M., 1993. Orthopyroxene-bearing, mafic migmatites at Cone Peak, California: evidence for the formation of migmatitic granulites by anatexis in an open system. Journal of Metamorphic Geology 11, 291–307.
Hildreth, W., Moorbath, S., 1988. Crustal contributions to arc magmatism in the Andes of central Chile. Contributions to Mineralogy and Petrology 98, 455–489.
Holland, J.E., Surpless, B., Smith, D., Loewy, S.L., Lackey, J.S., 2013. Intrusive history and petrogenesis of the Ash Mountain Complex, Sierra Nevada batholith, California (USA). Geosphere 9, 691–717. http://dx.doi.org/10.1130/GES00890.1.
Huffman, O.F., 1972. Lateral displacement of upper Miocene rocks and the Neogene history of offset along the San Andreas fault in central California. Geological Society of America Bulletin 83, 2913–2946. http://dx.doi.org/10.1130/0016-7606(1972)83[2913:LDOUMR]2.0.CO;2.
Ito, K., Kennedy, G.C., 1971. An experimental study of the basalt–garnet granulite–eclogite transition. Geophysical Monograph 14, 303–314.
Jacobson, C.E., Grove, M., Pedrick, J.N., Barth, A.P., Marsaglia, K.M., Gehrels, G.E., Nourse, J.A., 2011. Late Cretaceous-early Cenozoic tectonic evolution of the southern California margin inferred from provenance of trench and forearc sediments. Geological Society of America Bulletin 123 (3–4), 485–506. http://dx.doi.org/10.1130/B30238.1.
James, E.W., 1992. Cretaceous metamorphism and plutonism in the Santa Cruz Mountains, Salinian block, California, and correlation with the southernmost Sierra Nevada. Geological Society of America Bulletin 104, 1326–1339. http://dx.doi.org/10.1130/0016-7606(1992)104<1326:CMAPIT>2.3.CO;2.
James, E.W., Mattinson, J.M., 1988. Metamorphic history of the Salinian Block: an isotopic reconnaissance. In: Ernst, W.G. (Ed.), Metamorphism and Crustal Evolution of the Western United States, Rubey Series 7. Prentice-Hall, Old Tappan, N. J., pp. 938–952.
John, D., 1981. Structure and petrology of pelitic schist in the Fremont Peak pendant, northern Gabilan Range, California. Geological Society of America Bulletin 92 (no. 5), 237–246. http://dx.doi.org/10.1130/0016-7606 (1981)92<237:SAPOPS>2.0.CO;2.
Kay, R.W., 1978. Aleutian magnesian andesites: melts from subducted Pacific ocean crust. Journal of Volcanology and Geothermal Research 4, 117–132.
Kay, S.M., Gody, E., Kurz, A., 2005. Episodic arc migration, crustal thickening, subduction erosion and magmatism in the south-central Andes. Geological Society of America Bulletin 117, 67–88.
Kidder, S., Ducea, M.N., 2006. High temperatures and inverted metamorphism in the schist of Sierra de Salinas, California. Earth and Planetary Science Letters 241, 422–437. http://dx.doi.org/10.1016/j.epsl.2005.11.037.
Kidder, S., Ducea, M., Gehrels, G.E., Patchett, P.J., Vervoort, J., 2003. Tectonic and magmatic development of the Salinian Coast Ridge Belt, California. Tectonics 22. http://dx.doi.org/10.1029/2002TC001409.
Kidder, S.B., Herman, F., Saleeby, J., Avouac, J.-P., Ducea, M.N., Chapman, A.D., 2013. Shear heating not a cause of inverted metamorphism. Geology 41, 899–902. http://dx.doi.org/10.1130/G34289.1.
Kistler, R.W., 1990. Two different lithosphere types in the Sierra Nevada, California. Memoir Geological Society of America 174, 271–281.
Kistler, R.W., Champion, D.E., 2001. Rb–Sr whole-rock and mineral ages, K–Ar, $^{40}Ar/^{39}Ar$, and U–Pb mineral ages, and strontium, lead, neodymium, and oxygen isotopic compositions for granitic rocks from the Salinian Composite Terrane, California. U.S. Geological Survey Open-File Report 01–453 (84 pp.).
Kistler, R.W., Peterman, Z.E., 1978. Reconstruction of crustal blocks of California on the basis of initial strontium isotopic compositions of Mesozoic granitic rocks. United States Geological Survey Professional Paper 1071 (17 pp.).
Kistler, R.W., Chappell, B.W., Peck, D.L., Bateman, P.C., 1986. Isotopic variation in the Tuolumne Intrusive Suite, central Sierra Nevada, California. Contributions to Mineralogy and Petrology 94, 205–220. http://dx.doi.org/10.1007/BF00592937.
Lackey, J.S., Valley, J.W., Saleeby, J.B., 2005. Supracrustal input to magmas in the deep crust of Sierra Nevada Batholith; evidence from high-$\delta^{18}O$ zircon. Earth and Planetary Science Letters 235, 315–330.
Lackey, J.S., Valley, J.W., Chen, J.H., Stockli, D.F., 2008. Dynamic magma systems, crustal recycling, and alteration in the central Sierra Nevada Batholith: the oxygen isotope record. Journal of Petrology 49 (7), 1397–1426.
Lawson, A.C., 1893. The geology of Carmelo Bay. University of California Bulletin of the Department of Geology 1, 1–57.
Mamani, M., Worner, G., Sempere, T., 2010. Geochemical variations in igneous rocks of the Central Andean orocline (13 S to 18 S): tracing crustal thickening and magma generation through time and space. Geological Society of America Bulletin 122, 162–182.
Matthews III, V., 1976. Correlation of Pinnacles and Neenach volcanic fields and their bearing on San Andreas fault problem. The American Association of Petroleum Geologists Bulletin 60, 2128–2141.
Mattinson, J.M., 1978. Age, origin, and thermal histories of some plutonic rocks from the Salinian block of California. Contributions to Mineralogy and Petrology 67, 233–345.
Mattinson, J.M., 1990. Petrogenesis and evolution of the Salinian magmatic arc. In: Anderson, J.L. (Ed.), The nature and origin of Cordilleran magmatism. Geological Society of America Memoir, 174, pp. 237–250.
Matzel, J.E.P., Bowring, S.A., Miller, R.B., 2006. Time scales of pluton construction at differing crustal levels: examples from the Mount Stuart and Tenpeak intrusions, North Cascades, Washington. Geological Society of America Bulletin 118, 1412–1430. http://dx.doi.org/10.1130/B25923.1.
McCulloch, M.T., Gregory, R.T., Wasserburg, G.J., Taylor Jr., H.P., 1980. A neodymium, strontium and oxygen isotopic study of the Cretaceous Samail ophiolite and implications for the petrogenesis and seawater-hydrothermal alteration of oceanic crust. Earth and Planetary Science Letters 46, 201–211.
Miller, J.S., Glazner, A.F., Crowe, D.E., 1996. Muscovite–garnet granites in the Mojave Desert; relation to crustal structure of the Cretaceous arc. Geology 24 (4), 335–338.
Miller, J.S., Glazner, A.F., Farmer, G.L., Suayah, I.B., Keith, L.A., 2000. A Sr, Nd and Pb isotopic study of mantle domains and crustal structure from Miocene volcanic rocks of the Mojave Desert, California. Geological Society of America Bulletin 112, 1264–1279. http://dx.doi.org/10.1130/0016-7606(2000)112<1264:ASNAPI>2.0.CO;2.
Miller, R.B., Paterson, S.R., Matzel, J.P., 2009. Plutonism at different crustal levels: insights from the ~5–40 km (paleodepth) North Cascades crustal section, Washington. In: Miller, R.B., Snoke, A.W. (Eds.), Crustal Cross Sections from the Western North American Cordillera and Elsewhere: Implications for Tectonic and Petrologic Processes. Geological Society of America Special Paper, 456, pp. 125–149. http://dx.doi.org/10.1130/2009.2456(05).
Moyen, J.F., 2009. High Sr/Y and La/Yb ratios: the meaning of the “adakitic signature”. Lithos 112, 556–574. http://dx.doi.org/10.1016/j.lithos.2009.04.001.
Nutt, C.J., 1977. The Escondido Mafic–Ultramafic Complex: A Concentrically Zoned Body in the Santa Lucia Range, California. (M.S. thesis) Stanford University (90 pp.).
O'Brien, P.J., Rötzler, J., 2003. High-pressure granulites: formation, recovery of peak conditions and implications for tectonics. Journal of Metamorphic Geology 21, 3–20.
Otamendi, J.E., Ducea, M.N., Tibaldi, A.M., Bergantz, G., de la Rosa, J.D., Vujovich, G.I., 2009. Generation of tonalitic and dioritic magmas by coupled partial melting of gabbroic and metasedimentary rocks within the deep crust of the Famatinian magmatic arc, Argentina. Journal of Petrology 50, 841–873.
Otamendi, J.E., Ducea, M.N., Bergantz, G.W., 2012. Geological, petrological and geochemical evidence for progressive construction of an arc crustal section, Sierra de Valle Fértil, Famatinian Arc, Argentina. Journal of Petrology 53, 761–800. http://dx.doi.org/10.1093/petrology/egr079.
Page, B.M., 1982. Migration of Salinian composite block, California, and disappearance of fragments. American Journal of Science 282, 1694–1734.
Patchett, P.J., Ruiz, J., 1987. Nd isotopic ages of crust formation and metamorphism in the Precambrian of eastern and southern Mexico. Contributions to Mineralogy and Petrology 96, 523–528.
Paterson, S.R., Farris, D.W., 2008. Downward host rock transport and the formation of rim monoclines during the emplacement of Cordilleran batholiths. Transactions of the Royal Society of Edinburgh: Earth Sciences 97 (n. 4), 397–413 (Special Issue Plutons and Batholiths (The Wallace Pitcher Memorial Volume)).
Paterson, S.R., Okaya, D., Memeti, V., Economos, R., Miller, R.B., 2011. Magma addition and flux calculations of incrementally constructed magma chambers in continental margin arcs: combined field, geochronologic, and thermal modeling studies. Geosphere 7, 1439–1468. http://dx.doi.org/10.1130/GES00696.1.
Patino Douce, A.E., 1999. What do experiments tell us about the relative contributions of crust and mantle to the origin of granitic magmas? In: Castro, A., Fernandez, C., Vigneresse, J.L. (Eds.), Understanding Granites: Integrating New and Classical Techniques. Special Publications, 158. Geological Society, London, pp. 55–75.
Pickett, D.A., Saleeby, J.B., 1993. Thermobarometric constraints on the depth of exposure and conditions of plutonism and metamorphism at deep levels of the Sierra Nevada Batholith, Tehachapi Mountains, California. Journal of Geophysical Research 98, 609–629.
Pickett, D.A., Saleeby, J.B., 1994. Nd, Sr, and Pb isotopic characteristics of Cretaceous intrusive rocks from deep levels of the Sierra Nevada Batholith, Tehachapi Mountains,

California. Contributions to Mineralogy and Petrology 118 (no. 2), 198–215 (110.1007/BF01052869).
Rapp, R.P., Watson, E.B., 1995. Dehydration melting of metabasalt at 8–32 kbar; implications for continental growth and crust-mantle recycling. Journal of Petrology 36, 891–931.
Ratajeski, K., Sisson, T.W., Glazner, A.F., 2005. Experimental and geochemical evidence for derivation of the El Capitan Granite, California, by partial melting of hydrous gabbroic lower crust. Contributions to Mineralogy and Petrology 149, 713–734. http://dx.doi.org/10.1007/s00410-005-0677-4.
Ross, D.C., 1972. Petrographic and chemical reconnaissance study of some granitic and-gneissic rocks near the San Andreas fault from Bodega Head to Cajon Pass, California. United States Geological Survey Professional Paper 698 (92 pp.).
Ross, D.C., 1975. Modal and chemical data for granitic rocks of the Gabilan Range, central Coast Ranges, California. National Technical Information Service Report PB-242 458/AS (42 pp.).
Ross, D.C., 1978. The Salinian block-A Mesozoic granitic orphan in the California Coast Ranges. In: Howell, D.G., McDougall, K.A. (Eds.), Mesozoic paleogeography of the Western United States: Pacific Section, SEPM (Society for Sedimentary Geology). Pacific Coast Paleogeography Symposium, 2, pp. 509–522.
Ross, D.C., 1979. Maps showing sample localities and ternary plots and graphs showing modal and chemical data for granitic rocks of the Santa Lucia Range, Salinian Block, California Coast Ranges. U.S. Geological Survey Miscellaneous Field Studies Map MF-799 (16 pp.).
Ross, D.C., 1982. Results of instrumental neutron activation analyses for selected plutonic samples from the Salinian block, California Coast Ranges. U.S. Geological Survey Open-File Report 82–935 (17 pp.).
Ross, D.C., 1989. The metamorphic and plutonic rocks of the southernmost Sierra Nevada, California, and their tectonic framework. United States Geological Survey Professional Paper 1381 (159 pp.).
Rudnick, R.L., 1995. Making continental crust. Nature 378, 571–578.
Rudnick, R.L., Gao, S., 2003. Composition of the continental crust. In: Holland, H.D., Turekian, K.K., Rudnick, R.L. (Eds.), The Crust. Treatise on Geochemistry, 3. Elsevier, Pergamon, Oxford, pp. 1–64.
Saleeby, J.B., 1990. Progress in tectonic and petrogenetic studies in an exposed crosssection of young (~100 Ma) continental crust, southern Sierra Nevada, California. In: Salisbury, M.H. (Ed.), Exposed Cross Sections of the Continental Crust. D. Reidel Publishing, Dordrecht, pp. 132–158.
Saleeby, J., 2003. Segmentation of the Laramide slab: evidence from the southern Sierra Nevada region. Geological Society of America Bulletin 115, 655–668. http://dx.doi.org/10.1130/0016-7606(2003) 115<0655: SOTLSF>2.0.CO;2.
Saleeby, J., 2011. Geochemical mapping of the Kings-Kaweah ophiolite belt, California—evidence for progressive mélange formation in a large offset transform-subduction initiation environment. In: Wakabayashi, J., Dilek, Y. (Eds.), Mélanges: Processes of Formation and Societal Significance: Boulder, Colorado. Geological Society of America Special Paper, 480, pp. 31–73. http://dx.doi.org/10.1130/2011.2480(02).
Saleeby, J., Farley, K.A., Kistler, R.W., Fleck, R., 2007. Thermal evolution and exhumation of deep-level batholithic exposures, southernmost Sierra Nevada, California. In: Cloos, M., Carlson, W.D., Gilbert, M.C., Liou, J.G., Sorensen, S.S. (Eds.), Convergent Margin Terranes and Associated Regions: A Tribute to W.G. Ernst. Geological Society of America Special Paper, 419, pp. 39–66. http://dx.doi.org/10.1130/2006.2419(01).
Schott, R.C., Johnson, C.M., 1998. Sedimentary record of the Late Cretaceous thrusting and collapse of the Salinia–Mojave magmatic arc. Geology 26, 327–330. http://dx.doi.org/10.1130/0091-7613(1998) 026<0327:SROTLC>2.3.CO;2.
Schott, R.C., Johnson, C.M., O'Neil, J.R., 2004. Late Cretaceous tectonic history of the Sierra–Salinia–Mojave arc as recorded in conglomerates of the Upper Cretaceous and Paleocene Gualala Formation, northern California. Journal of Geophysical Research 109, B02204. http://dx.doi.org/10.1029/2003JB002845.
Sharman, G.R., Graham, S.A., Grove, M., Hourigan, J.K., 2013. A reappraisal of the early slip history of the San Andreas fault, central California, USA. Geology 41 (no. 7), 727–730. http://dx.doi.org/10.1130/G34214.1.
Silver, L.T., Chappell, B.W., 1988. The Peninsular Ranges Batholith: an insight into the evolution of the Cordilleran batholiths of southwestern North America. Transactions of the Royal Society of Edinburgh, Earth Science 79, 105–121.
Stern, C.R., 1991. Role of subduction erosion in the generation of Andean magmas. Geology 19, 78–81.
Sun, S.S., McDonough, W.F., 1989. Chemical and isotopic systematics of oceanic basalts; implications for mantle composition and processes. In: Saunders, A.D., Norry, M.J. (Eds.), Magmatism in the Ocean Basins. The Geological Society of London Special Publication, 42, pp. 315–345.
Tepper, J.H., Nelson, B.K., Bergantz, G.W., Irving, A.J., 1993. Petrology of the Chilliwack batholith, North Cascades, Washington: generation of calc-alkaline granitoids by melting of mafic lower crust with variable water fugacity. Contributions to Mineralogy and Petrology 113, 333–351.
Trask, P.D., 1926. Geology of Point Sur Quadrangle, California. University of California Publications in Geological Sciences 16 (6), 119–186.
Vedder, J.G., Howell, D.G., McLean, H., 1982. Stratigraphy, sedimentation, and tectonic accretion of exotic terranes, southern Coast Ranges, California. AAPG Memoir 34, 471–496.
von Huene, R., Scholl, D.W., 1991. Observations at convergent margins concerning sediment subduction, subduction erosion, and the growth of continental-crust. Reviews of Geophysics 29, 279–316.
Wetmore, P., Ducea, M.N., 2011. Geochemical evidence of a near-surface history for source rocks of the central Coast Mountain Batholith, British Columbia. International Geology Review 53, 230–260. http://dx.doi.org/10.1080/00206810903028219.
Wiebe, R.A., 1966. Structure and Petrology of Ventana Cones Area, California. [Ph.D. thesis] Stanford University (95 pp.).
Wiebe, R.A., 1970. Pre-Cenozoic tectonic history of the Salinian Block, western California. Geological Society of America Bulletin 81, 1837–1842. http://dx.doi.org/10.1130/0016-7606(1970) 81[1837:PTHOTS]2.0.CO;2.
Wolf, M.B., Wyllie, P.J., 1994. Dehydration-melting of amphibolite at 10 kbar; the effects of temperature and time. Contributions to Mineralogy and Petrology 115, 369–383.
Wood, D.J., Saleeby, J.B., 1997. Late Cretaceous–Paleocene extensional collapse and disaggregation of the southernmost Sierra Nevada Batholith. International Geology Review 39 (11), 973–1009. http://dx.doi.org/10.1080/00206819709465314.
Wooden, J.L., Stacey, J.S., Howard, K.A., Doe, B.R., Miller, D.M., 1988. Pb isotopic evidence for the formation of Proterozoic crust in the Southwestern United States. In: Ernst, W.G. (Ed.), Metamorphism and Crustal Evolution of the Western United States, Rubey. vol. 7. Prentice-Hall, Old Tappan, N. J, pp. 68–86.
Wyllie, P.J., 1984. Constraints imposed by experimental petrology on possible and impossible magma sources and products. Philosophical Transactions of the Royal Society of London, Series A 310, 439–456.
Wyllie, P.J., Wolf, M.B., 1993. Amphibolite dehydration melting: sorting out the solidus. In: Prichard, H.M., et al. (Eds.), Magmatic Processes and Plate Tectonics. Geological Society of London Special Publication, 76, pp. 405–416.
Zartman, R.E., 1974. Lead isotopic provinces in the Cordillera of the western United States and their significance. Economic Geology 69, 792–805.
Zeng, L., Saleeby, J.B., Asimow, P., 2005. Nd isotope disequilibrium during crustal anatexis: a record from the Goat Ranch migmatite complex, southern Sierra Nevada batholith, California. Geology 33, 53–56.